Charge Transport in Disordered Organic Materials and Its Relevance to Thin-Film Devices: A Tutorial Review

ARTICLE *in* ADVANCED MATERIALS · JULY 2009

Impact Factor: 17.49 · DOI: 10.1002/adma.200803541

4 AUTHORS, INCLUDING:

Nir Tessler
Technion - Israel Institute of Technology
198 PUBLICATIONS **7,845** CITATIONS

Charge Transport in Disordered Organic Materials and Its Relevance to Thin-Film Devices: A Tutorial Review

By *Nir Tessler,* Yevgeni Preezant, Noam Rappaport,* and *Yohai Roichman*

Semiconducting polymers and small molecules form an extremely flexible class of amorphous materials that can be used in a wide range of applications, some of which are display, radio-frequency tags, and solar cells. The rapid progress towards functional devices is occurring despite the lack of sufficient understanding of the physical processes and very little experience in device engineering. This tutorial review aims to provide sufficient intuitive background to draw more researchers to look into the fundamental aspects of device physics and engineering.

1. General Introduction

In this review, we describe a variety of models or theoretical approaches to transport in disordered media and discuss the implication to modern organic devices. There are far too many models or variations, so our aim is not to try to cover them all. Instead, we show that when the different models are presented along with the assumptions included while being developed, they can all teach us and help us to develop some intuition regarding what goes on in nonordered materials. One may encounter debates regarding a model being wrong, but it is our belief that only when the models are used out of context (not within their basic assumptions) the obtained results could be false.

One of the things one encounters while starting to study organic semiconductors is that the textbook models taught in semiconductor-device courses have to be revisited, and one has to look for ''old'' books that were written before silicon technology took over. With this spirit, we start a few years back, or a century ago. In 1900, three years after the discovery of the electron by Thomson, Drude proposed a model that explained the known conductivity phenomenon in metals and other types of materials.[1] This model was based on the assumption that electrons classically accelerate under an applied electric field and collide with the lattice's heavy positive ions. Upon collision, the electrons were assumed to scatter into a random angle and at a speed that was on average consistent with the local temperature. It would then go on accelerating until the next scattering event. This model, although erroneous in the assumption that the basic scattering centers were the lattice ions, was able to physically explain the already known Ohm's law and the Joule heating effect. Along with the debut of quantum mechanics came the quantum mechanical description of matter and the realization that in a well-ordered lattice electrons should be mathematically described as Bloch waves, and that the scattering was not the result of collisions with any lattice ion but rather scattering from defects, contaminations, and phonons. Nevertheless, the Drude model, under the semiclassical approximation, is conceptually appropriate for describing electron transport through crystal lattices, that is, freely roaming charge carriers that scatter upon collisions with defects, contaminations, and phonons. The carriers earn the name ''free'' whenever the material properties are such that the mean free path between collisions, L, is much longer than the typical carrier's Bloch wavelength, thus the carriers have very broad wavefunctions extending over many lattice units.

However, as was historically elucidated by Anderson,[2] introducing disorder into the lattice and breaking the crystal symmetry results in the wavefunctions becoming localized and in the formation of energy states in the forbidden band-gap. The Drude concepts, and others deriving on its intuitive approach, can no longer serve us in explaining transport under such circumstances. Since the materials we are interested in are disordered in nature, we shall devote the discussion to some phenomena and physical theories relating to the transport of charge carriers through disordered media. As stated at the beginning, we do not aim to cover all existing theories or variations, but rather discuss only those that would help in developing some intuitive understanding of the transport in amorphous organic materials.

The discussion in the following section starts in an abstract mode, so to help the reader place it in the right context we outline, briefly, how one could represent a film of conjugated polymers (or molecules) by a map of sites a charge would go through while drifting with the electric field. Figure 1a shows schematically a distribution of conjugated polymer chains as might be found in a small section of a polymer film. It is well known that the conjugated polymer is not a single electronic wire but that it is rather broken into subunits (by chemical or physical defects) that are called conjugation units, and the number of monomers making this unit is called the conjugation length. Figure 1b shows how the polymer chains would be broken into subconjugation units. Namely, we have now many small electronic units that can also be thought of as small molecules distributed across the film. The ''only'' role that was played by the polymer chain was to

[*] Prof. N. Tessler, Y. Preezant, Dr. N. Rappaport, Dr. Y. Roichman
Electrical Engineering Department
Nanoelectronic Center
Technion, Haifa 32000 (Israel)
E-mail: nir@ee.technion.ac.il

DOI: 10.1002/adma.200803541

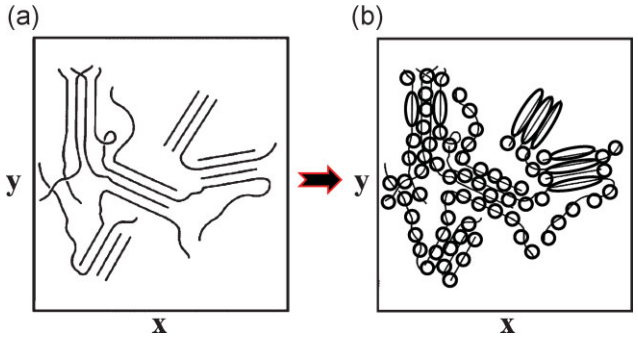

Figure 1. a) Schematic description of polymer chains. b) Illustration of how a long chain would break into small conjugation units (or sites).

determine the distribution of the units (''molecules'') in the film that is part of the film morphology.

Having simplified the film into an ensemble of electronic sites, we can ''forget'' that we had polymers or molecules and consider that we have a distribution of sites that can host charge and enable it to move across a film. As Figure 2 shows, we need now to analyze charge transport across sites that are distributed in real space (Fig. 2a) as well as in energy space (Fig. 2b). The solid line in Figure 2 illustrates an imaginary path a charge might take while crossing the film.

2. Charge Motion in Disordered Organic Materials

As we have already mentioned, in well-ordered materials transport is essentially modeled by application of the semi-classical approximation and the Drude model. There exists a simple exception to this picture, where the role of trap states in the forbidden gap is included. In that case, the transport is essentially ideal, that is, only that at a given time a certain percentage of the carriers are considered to be trapped in localized states, and are therefore static and not contributing to the current.[3] This changes the relation between the voltage and the current, but does not change the concept of how the carriers are transported. The conceptual leap in understanding transport in disordered media is in realizing that current can also be the result of charge transport through localized states.

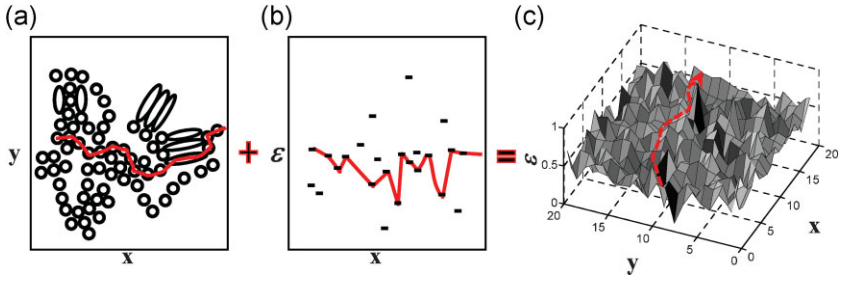

Figure 2. Schematic description showing that the transport sites are distributed both a) in space and b) in energy. c) A schematic 2D map of a rough energy surface. The line describes a hypothetical path a charge might take while hopping from one side of the sample to the other (under applied electric field).

Nir Tessler received his B.Sc. summa cum laude in Electrical Engineering at Technion Israel Institute of Technology. After ''falling in love'' with organic optoelectronics he strived to contribute to the understanding that organics can be used in numerous applications where the latest example was of polymer based LEDs emitting at telecom wavelengths. In 1999, he joined the Technion as a faculty member studying new materials, device design and analysis, and charge transport and related phenomena in disordered amorphous materials based devices.

Three essential depictions are given in Figure 3 for the nature of the relevant states in the material. The filled areas in the figure signify that the states are localized. In Figure 3a the localized states are shown to reside in the forbidden band-gap between the free carrier bands. This scenario is similar to what has been mentioned above, where depending on the relative position of the traps and their density they may be deep or shallow. Figure 3b shows a scenario where the trap states comprise the lower part of the whole conduction band with an energy E_M (the mobility edge), beyond which the states are unlocalized. This is more like a shallow-trap situation. In Figure 3c the entire band is comprised of localized states. Under the first two circumstances, the current will most likely (although not necessarily) be dominated by the unlocalized carriers; however, in the third case that cannot be true.

One may suppose that if all carriers occupy states that are localized, then the material should invariably be considered an insulator. However, localized charge carriers may travel through the material by hopping from one localized state to the next. The rate at which this occurs is related to the conductivity of the material, and in some cases also to the concept of mobility. A carrier may hop from one site to the next provided the site of origin is occupied by a carrier and the target site can accept additional carrier (typically this means that the target site is unoccupied). Therefore, in order to describe this process, a probability evolution equation is needed, known as the master equation:

$$\frac{\partial}{\partial t} f_i(t) = -\sum_{j \neq i} W_{ji} f(t)[1 - f_i(t)] + \sum_{j \neq i} W_{ij} f_j(t)[1 - f_i(t)] - \lambda_i f_i(t) \quad (1)$$

In Equation 1 $f_i(t)$ is the probability that site i (at location R_i and energy ε_i) is occupied by a carrier or excitation at time t (therefore $[1 - f_j(t)]$ is the probability that site j is unoccupied), W_{ij} is the transition rate from site i to site j, and λ_i is the decay rate of the

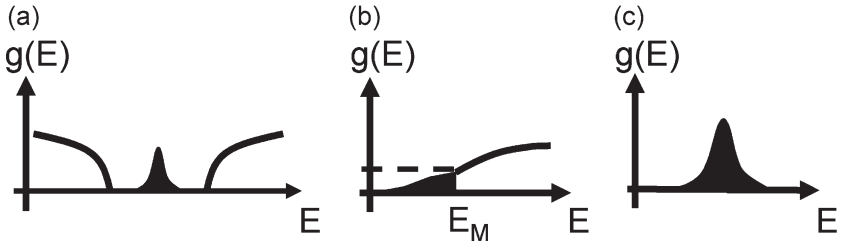

Figure 3. Different scenarios for the setting of traps in relation to the general density of states—a) in the forbidden band-gap isolated from the main bands, b) edge portion of one of the bands with a typical mobility edge energy (E_M) beyond which the states are free, c) and a completely localized band.

excitation at site *i*. This is a nonlinear equation with a potentially extremely large number of terms. For a given problem, the site locations $\{R_i\}$ need be given as well as the decay rates for each site (often one assumes that recombination is only a small perturbation, and assumes that $\lambda_i = 0$). Two popular expressions for the W_{ij} transition rates were given by Anderson (what is known in the organic semiconductor field as the Miller–Abrahams expression) and by Mott.[4] The Miller–Abrahams expression[5,6] is based on a phonon-assisted tunneling mechanism, and is given by:

$$W_{ij} = \upsilon_0 \exp(-2\gamma|\mathrm{R_{ij}}|)\begin{cases} \exp\left(-\dfrac{(\varepsilon_\mathrm{j}-\varepsilon_\mathrm{i})}{\kappa \mathrm{T}}\right) & \forall \varepsilon_\mathrm{j} > \varepsilon_\mathrm{i} \\ 1 & \text{else} \end{cases} \quad (2)$$

where υ_0 is the phonon vibration frequency (can be intuitively understood as the ''jump-attempt'' rate or simply taken as a normalization factor), γ is the inverse localization radius (the result of the overlap integral of the wavefunctions assuming exponential decay with distance), and ε_i and ε_j are the energy levels of the respective sites. In this model, no relaxation of the local site configurations (the polaronic effect) is accounted for. The second popular approach for expressing the transfer rate is based on the polaronic effect, which describes the coupling between the molecule configuration (physical structure) and its electronic energy. In this case, the (two) molecules involved in the charge transfer (or chemical reaction) should first assume a configuration in which the total energy is indifferent to the charge being on one molecule or the other. In some sense, one may say that the charge transfer would occur when the molecular states involved are at resonance. Namely, charge carrier may hop from one site to another given that a favorable configuration is reached (the chances for which are temperature dependent). The resulting expression from this analysis is:[4]

$$W_{ij} = \frac{J^2}{\hbar}\frac{\pi}{\sqrt{2U_\mathrm{b}kT}}\exp\left(-\frac{U_\mathrm{b}}{2kT}\right) \exp\left(-\frac{(\varepsilon_j-\varepsilon_i)}{2kT}-\frac{\beta(\varepsilon_j-\varepsilon_i)^2}{8kTU_\mathrm{b}}\right) \quad (3)$$

where J is related to the overlap integral and is given by $J^2 = J_0^2\exp(-2\gamma|R_{ij}|)$ with J_0 calculated from the crossing point between the reactant and product curves[7] and U_b is the polaron binding energy.

Although the energy dependence of the transfer rate is very different between the Miller–Abraham's (M.A.) and the polaronic one (see Fig. 4), under steady-state and quasi-equilibrium (low E field) conditions there is no real difference between the transport (current) derived from Equations 2 and 3, but for the additional activation energy associated with the polaron binding energy. There is however, an inherent difference, relevant to steady-state conditions, which does not appear in these equations and has to do with the fact that the most favorable configuration at which charge transfer occurs is one that can be accessed through the phonons (vibration types) present in the system (in the solid, the relevant vibrations are both intra- and intermolecular). As the temperature goes down, the relative occupation of different vibration changes, and at some temperature (~half of the significant ''phonon temperature'') the ''high-temperature favorable configuration'' cannot be reached through the existing vibrations, and a new ''low-temperature favorable configuration'' is chosen. For this new configuration, the tunneling is much slower, but as it requires less energy to be reached, it is associated with lower activation energy. We have not been able to find direct measurements of the phonon temperature associated with the charge transport, but the one associated with exciton emission in conjugated polymers is in the range of 300–500 K.[8,9] Namely, in most temperature-dependent measurements this effect will be highly influential, and may mask the effects that are dominant in hard materials. We will come back to the issue of polaronic transfer rate in the context of nonequilibrium transport further ahead in this paper.

Regardless of the transfer rate of choice, one has to find a solution for Equation 1. There are several approaches to handling this equation in order to arrive at useful results. In many cases, this requires the linearization of Equation 1 by either assuming a dilute system (low density) of uncorrelated particles, and thus eliminating the terms $[1-f_i(t)]$ and/or by assuming small deviations from equilibrium, and thus the overall rates are linear

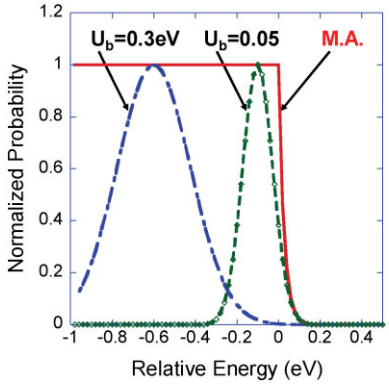

Figure 4. The transfer rate as a function of the energy difference between initial and final states (negative = going down in energy) for the Miller–Abraham's and polaronic rates (shown for binding energies of 0.05 and 0.3 eV).

with the difference in electrochemical potential (quasi-Fermi level). Next, in Section 3, we briefly outline some semi-phenomenological models that are based on the basic equations above. This will be followed in Section 4 with more computer-intensive models.

2.1. Behind the Scenes

Throughout the paper we will try to draw you attention to "hidden" assumptions. For example, the rates described above and the entire discussion in this contribution assumes that once a carrier hops to a state it thermalizes on that state instantaneously (there is also a short discussion of thermalization length in Section 6.3).

3. Semi-Phenomenological Models for System Conductivity

Most of the semi-phenomenological models were not developed with organic (soft) materials in mind, so one may ask why we should be considering them here. The best way we can answer such a question is illustrated in Figure 5.

3.1. Mott's Variable Range Hopping

In the following, we try to illustrate Mott's intuitive approach.[10] As Equation 1 shows, for efficient hopping to occur, the initial state must be occupied and the final state be empty. Mapping/finding these sites in real space is not trivial, due to the large disorder, but in energy space it is sometimes much easier.

As is illustrated in Figure 6a, it is natural to expect that charges would hop at an energy band around the Fermi level, where filled and empty states are closest. To ensure that this is strictly true, we assume in the following that the site energy distribution, $\rho(\varepsilon)$, is uniform ($\rho(\varepsilon) = \rho$ in Fig. 6b). For such a uniform distribution of states, the only distinction can be introduced by the Fermi distribution, and hence the transport would take place close the Fermi level.

To be able to characterize this transport, we need to know how large the band that carriers make use of while hopping, $\Delta\varepsilon$, is. If

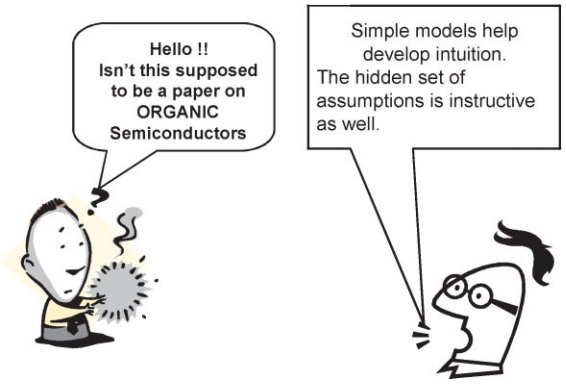

Figure 5. The reason why one should examine classical "inorganic" models.

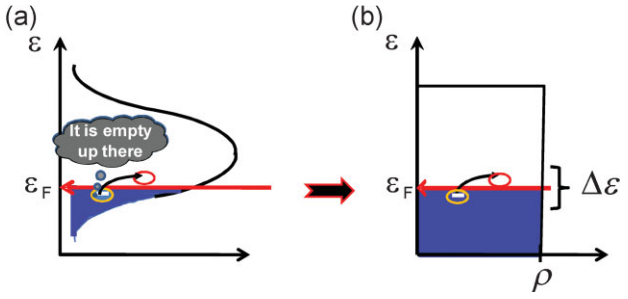

Figure 6. a) Illustration of charges occupying the lower-energy part of a Gaussian density of states. The picture also shows a charge ready to hop upwards in energy toward an empty state. b) Simplified DOS we will use for the discussion of Mott's variable range hopping.

the width is very small, then the density of sites that are of energy within this band ($\rho\Delta\varepsilon$) is going to be very small, and hence on average the sites would be very distant from each other, thus rendering the tunneling probability negligible. On the other hand, if we try to minimize the average distance by making the energy-band width very large, then the penalty for using this width ($\sim\exp[-\Delta\varepsilon/kT]$) would diminish the probability of hopping. It is thus clear that there is an optimum value to be found in between these two extremes. When a carrier hops up by energy of $\Delta\varepsilon$ and over a distance R, it has practically $\frac{4}{3}\pi R^3\rho\Delta\varepsilon$ sites to choose from (ρ is the site density per unit energy). To ensure that a hop can occur, we require that a target site exist within range of (R, $\Delta\varepsilon$):

$$\frac{4}{3}\pi R^3\rho\Delta\varepsilon \cong 1 \tag{4}$$

Under these conditions, we can write the transition rate for moving in space while going up in energy as:

$$W_{ij} = \upsilon_0\exp(-2\gamma|R_{ij}|)\exp\left(\frac{\varepsilon_j-\varepsilon_i}{kT}\right) = \upsilon_0\exp\left(-2\gamma R - \frac{1}{kT\frac{4}{3}\pi R^3\rho}\right) \tag{5}$$

where we used Equation 4 in the right-hand side of Equation 5. In order to characterize the most probable hops a carrier would take, we need to find the distance (or energy band) that would result in the maximum rate, and we do that by taking the differential with respect to R:

$$\frac{\mathrm{d}W(R)}{\mathrm{d}R} = 0$$

or:

$$R^4_{\text{optimum}} = \frac{1}{8\gamma k\pi\rho}\frac{1}{T} \text{ or } \Delta\varepsilon_{\text{optimum}} = \frac{(8\gamma\kappa T)^{3/4}}{\frac{4}{3}(\pi\rho)^{0.25}} \tag{6}$$

Substituting Equation 6 into 5, we find:

$$W_{ij}|_{\max} = \upsilon_0 \exp\left(-\gamma\left(\frac{1}{8\gamma\kappa\pi\rho}\frac{1}{T}\right)^{1/4} - \frac{1}{\kappa T\frac{4}{3}\pi\left(\frac{1}{8\gamma\kappa\pi\rho}\frac{1}{T}\right)^{3/4}\rho}\right)$$

or

$$W_{ij}|_{\max} \propto \exp\left[-\left(\frac{T_0}{T}\right)^{1/4}\right] \quad (7)$$

which is Mott's famous variable-range hopping formula.

3.1.1. Behind the Scenes

In the above, we balanced, on behalf of the charge, tunneling (1st term in Eq. 5) with thermal activation (2nd term in Eq. 5), and to do so we assumed: i) "meaningful" hops are upward (by "meaningful" we mean in terms of contributing to the electronic current; we tend to consider that the carriers reside primarily at low energies, and that to propagate they need to hop up, to an empty state); ii) hops occur at the vicinity of the Fermi energy; iii) ρ is constant (at least around the Fermi energy) and/or that only small part of the DOS is being used/sampled by the charge carriers; iv) at the end, what we found is the width of the energy band ($\Delta\varepsilon$) through which a charge would hop. It is also instructive to estimate the optimum (average) jump distance according to Equation 6: assuming $\gamma = \mathrm{nm}^{-1}$, $kT = 0.026$, and $\rho = 10^{21}\,\mathrm{cm}^{-3}\,\mathrm{eV}^{-1}$, we find $R \cong 1\,\mathrm{nm}$ and $\Delta\varepsilon \cong 0.2\,\mathrm{eV}$.

To visualize the ideas of carriers residing near the Fermi level (E_F) and hopping through higher energies, we plot the charge density and current density as a function of energy for two exponential density-of-states (DOS) functions $\left(\mathrm{DOS} = \rho(\varepsilon) = \frac{N_t}{kT_0}\exp\left(-\frac{\varepsilon}{kT_0}\right)\right)$, one being steeper than $2kT$ ($T = 300\,\mathrm{K}$) and the other being shallower. The calculation is performed using the energy-space master equation model[11] that is discussed in Section 4. Figure 7a describes the case for a relatively more uniform DOS, and it shows that the charge density is indeed residing close to the Fermi level (E_F), and that the current is flowing mainly through states that are located just above the charge distribution (similar to Fig. 6). Figure 7b was calculated for a steeper DOS and it shows that in such a case the current would flow through much higher energies, where significantly more states are available.[12]

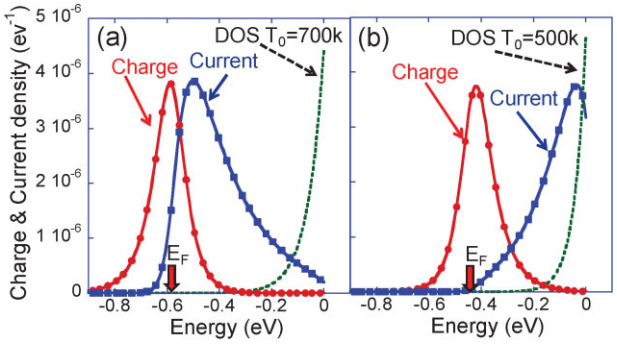

Figure 7. Normalized charge density, current density, and density of states for exponential DOS of a) $T_0 = 500\,\mathrm{K}$ and b) 700 K. In both cases, the filling factor of the DOS is 10^{-4} and the position of the relevant Fermi levels are marked with a thick arrow.

3.2. Ambegaokar's Percolation Approach

Following Mott's intuitive derivation, there were many attempts to cast more rigor into the final result, and one of the important contributions was by Ambegaokar et al.,[13] which suggested casting the charge transport as a percolation problem. The very basic notion that was governing the description above of Mott's VRH is that when a charge moves from one side of the sample to the other, it would try to do that using the fastest route (the "lazy-charge principle"). A similar situation is found in the case of water going, or percolating, through dry land. As percolation theory is very advanced, if we can find some physical justification for using it to solve charge transport it is a guaranteed home-run.

Before continuing, a few words about percolation or what it (in most cases) means. Let us assume we have a grid like paper (Fig. 8, left) and a thick black pen. We now pick at random a square on the page and randomly mark one of its sides. At first there would be only isolated lines (bonds) and later we would start to see a network of line starting to form. At some stage we would start to identify clusters and once a certain number of lines have been marked we would be able to find a continuous path going from top to bottom across the page. Once the two sides are connected we say that the system is at percolation threshold. Obviously, if we continue to draw lines, the connectivity between the two sides of the paper will strengthen. Most theories are concerned with what governs the formation of the threshold (as number of bonds, p, required) and they are concerned with infinite size systems where the conclusions made have a universal nature.

However, as we will see, the intuitive assumptions are still needed for casting charge transport onto the percolation problem.

The first stage in casting the transport onto a percolation problem is typically to go from a hopping system to a resistor network by turning the hopping rates into equivalent resistors (conductors).[13–15] To do so, the current between two sites can be written as $I_{ij} = q[w_{ij}f_i(1-f_j) - w_{ji}f_j(1-f_i)]$, and under small changes in the chemical potential (quasi-Fermi levels) between the two sites (due to applied bias) one can approximate it as:[13,14] $I_{ij} \approx G_{ij}(E_{Fj} - E_{Fi})$. For example, the derivation in Refs.[13,15] leads

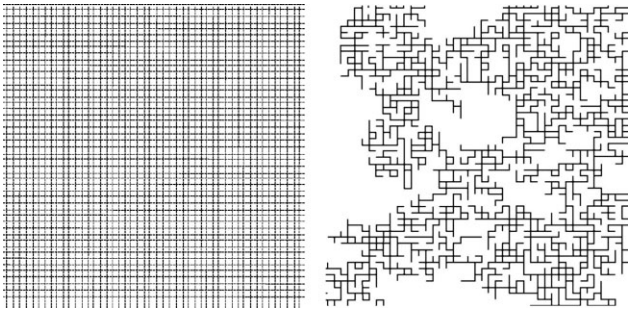

Figure 8. Left: a rectangular grid template. Right: example of bond percolation on a square grid produced by marking at random only one side of a small square at a time.

to (under the assumption that $|\varepsilon_j - E_F|; |\varepsilon_i - E_F|; |\varepsilon_j - \varepsilon_i| > kT$):

$$G_{ij} \approx \frac{q\upsilon_0}{kT}\exp(-2\gamma|R_{ij}|) \exp\left(-\frac{|\varepsilon_j - E_F| + |\varepsilon_i - E_F| + |\varepsilon_j - E_i|}{2kT}\right) \quad (8)$$

This expression shows that sites that are far from the Fermi level are connected through a relatively high resistor, and hence only sites close to the Fermi level would contribute to conduction through the resistor network. Note that in the derivation of Equation 8 one does not account for a situation where the density of states could be high at certain energy, such that the distance to a site in that energy range would be small enough to favor it over sites at other energies. Namely, we assume the density distribution to be uniform and, not surprisingly, we arrive at Mott's conclusion that the hopping is at or around the Fermi level.

So now we know how to move from Figure 9a to b, but we still do not know how to compute the conductivity of the system or at least its functional form (up to a normalization factor). This is where we expect the percolation theory to come in our aid, and for that to happen we need to represent the system as being at percolation threshold. To do so, one needs to be able to find the critical or typical conductance (G_C) that governs the conductivity of the system. The motivation is that conductance path that is of lower value would not be used since an alternative (parallel) path would be taken (Fig. 9c and the "lazy charge principle"). Namely, to go from one side of the sample to the other we need to use only conductance paths of values equal or larger than G_C. Moreover, conductance of higher value would not matter much, and can be considered as short-circuit (Fig. 9d), such that G_C is said to contain all the functional behavior of the entire network (the above arguments are only valid if the system is dilute enough so that the spread of resistance values is large and G_C is significantly set apart from the nearest lower and higher conductance values).

We can build such a system, of values only higher than G_C, by arranging all conductance paths according to their conductivity value and adding them to the network (at the proper place) one by one starting from the highest value. The moment a continuous path is formed across the sample, we stop and define the last value added as G_C. This is a classical critical-path percolation problem, and percolation theory can now be used to tell us that by the time we arrive at G_C we will have used a given fraction of the network (ϕ) such that at percolation threshold the following relation holds:

$$\frac{N_P}{N_S} = \phi \quad (9)$$

where N_P is the density of bonds (conduction paths) and N_S is the number of sites (grid points) in the percolating network. ϕ is a constant derived from numerical simulations of percolation problems.

To present Equation 9 in terms of the resistor network parameters, we note first that the density of sites (N_S) in the network is equivalent to $\rho 2\varepsilon_{Max}$. Second, as the typical length between connected sites is R_{Max}, a unit volume for a conducting path is of the order of $R_{Max}{}^3$, and hence the density of conducting paths (N_P) in the 3D network is proportional to $1/R_{Max}^3$. This leads to:

$$R_{Max}^3 \rho 2\varepsilon_{Max} = \theta \quad (10)$$

where Equation 10 is similar to Equation 4. To compute either [R_{Max}, ε_{Max}] or [N_P, N_S], one uses Equation 8 to relate the critical conductance G_C to the maximum hopping distance and the maximum hopping energy:

$$\begin{cases} G_C = \frac{q\upsilon_0}{kT}\exp(-2\gamma R_{Max}) \\ G_C = \frac{q\upsilon_0}{kT}\exp\left(-\frac{\varepsilon_{Max}}{kT}\right) \triangleq G_0\exp\left(-\frac{\varepsilon_C}{kT}\right) \end{cases} \quad (11)$$

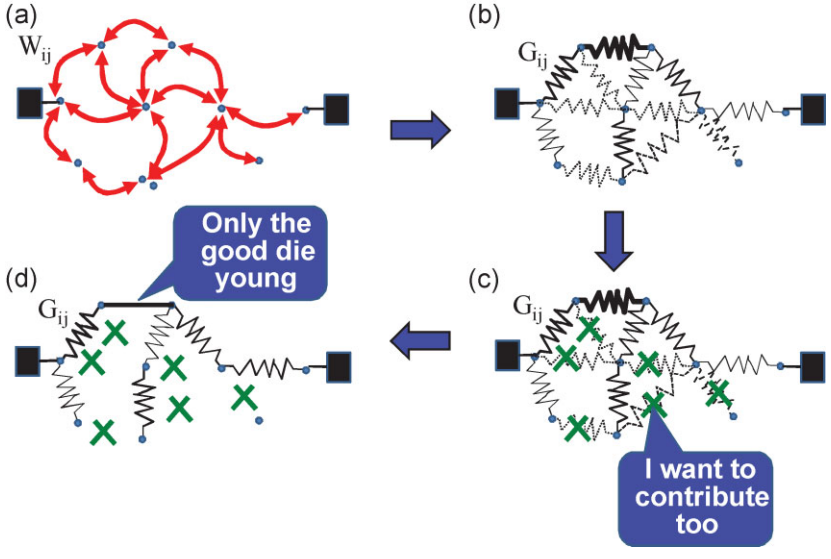

Figure 9. Schematic description of turning a) a hopping system into b) a resistor network. Next, we choose only the highest conductors that are required to keep the system continuous between left and right (c). d) We remove the lower-value conductors and are left with what is called the percolating network.

3.2.1. Behind the Scenes

In the above derivation, it is first of all assumed that the charges are hopping close to the Fermi energy, which is correct when the density of states is changing slowly with energy. Next, we assume that the full network is dilute and infinite in size, such that the critical path percolation theory is applicable (by dilute we mean $\gamma^{-1} \ll N^{1/3}$ where N is the total density of states).

3.3. Non-Uniform DOS

When we deal with non-uniform DOS, we need to check the two strong assumptions that were justified above for the uniform DOS:

1) Transport energy is close to, or at, the Fermi energy.
2) Site density at the Fermi energy is independent of the charge density.

3.3.1. Effective Transport Energy

The approach of computing transport energy[16,17] mainly addresses the effect of the shape of the DOS on the energy band through which the transport is occurring. In the context of organic semiconductors, the notion of effective transport energy was used by Arkhipov et al.,[18] who applied this theory to Gaussian DOS, and Martens et al.,[19] who developed a DOS-independent formalism. However, it is much simpler to illustrate this concept of transport energy using exponential DOS of the form:

$$\mathrm{DOS} = \rho(\varepsilon) = \frac{N_t}{kT_0}\exp\left(-\frac{\varepsilon}{kT_0}\right) \tag{12}$$

where N_t it the total density, T_0 is a characteristic temperature, and ε is the energy that is written as positive going downwards. As in the VRH derivation above, we are mainly interested in upward hops, and wonder where the electrons are hopping to. We start with the Miller–Abraham rate for hopping up in energy ($\varepsilon \rightarrow \varepsilon_j; \varepsilon_j < \varepsilon_i$):

$$\nu(\varepsilon_j) = \nu_0 \exp\left[-2\gamma R(\varepsilon_i, \varepsilon_j) - \frac{\varepsilon_i - \varepsilon_j}{kT}\right] \tag{13}$$

Just as in our above derivation of Mott's VRH, $R(\varepsilon_I, \varepsilon_j)$ is found from the density of the sites between ε_j and ε_i:

$$R_{ij}|_{(\varepsilon_i>\varepsilon_j)} = \left[\frac{4\pi}{3}\int_{\varepsilon_j}^{\varepsilon_i}\rho(\varepsilon)\mathrm{d}\varepsilon\right]^{-1/3} \tag{14}$$

Unlike the uniform DOS case, Equation 14 does not represent a simple straight-forward expression. To simplify it, one assumes that the DOS is highly non-uniform, or that it is steep enough that the number of sites beyond (below) ε_i is negligible compared to the number of those between ε_i and ε_j (for the exponential DOS it requires $(\varepsilon_i – \varepsilon_j) > 2kT_0$). Using this approximation:

$$\begin{aligned} R_{ij}|_{(\varepsilon_i>\varepsilon_j)} &\simeq \left[\frac{4\pi}{3}\int_{\varepsilon_j}^{\varepsilon_i}\rho(\varepsilon)\mathrm{d}\varepsilon\right]^{-1/3} \approx \left[\frac{4\pi}{3}\int_{\varepsilon_j}^{\infty}\rho(\varepsilon)\mathrm{d}\varepsilon\right]^{-1/3} \\ &= \left[\frac{4\pi}{3}\int_{\varepsilon_j}^{\infty}\frac{N_t}{kT_0}\exp\left(-\frac{\varepsilon}{kT_0}\right)\mathrm{d}\varepsilon\right]^{-1/3} \\ &= \left[\frac{4\pi}{3}N_t\exp\left(-\frac{\varepsilon_j}{kT_0}\right)\right]^{-1/3} \end{aligned} \tag{15}$$

And inserting Equation 15 into 13:

$$\nu(\varepsilon_j) = \nu_0\exp\left[-2\gamma\left(\frac{4\pi}{3}N_t\right)^{-1/3}\exp\left(\frac{\varepsilon_j}{3kT_0}\right) - \frac{\varepsilon_i - \varepsilon_j}{kT}\right] \tag{16}$$

To find where to the most probable hops are occurring, we look for the maximum of $\nu(\varepsilon_j)$:

$$\frac{\mathrm{d}\nu(\varepsilon_j)}{\mathrm{d}\varepsilon_j} = 0$$

and find that independent of the starting energy (ε_i), all hops will end up at:

$$\varepsilon_j = 3kT_0\ln\frac{3kT_0\left(\frac{4\pi}{3}N_t\right)^{1/3}}{2kT\gamma} \triangleq \varepsilon_t \text{ or } R|_{(\varepsilon_i\rightarrow\varepsilon_t)} \approx \frac{3T_0}{2T\gamma} \tag{17}$$

Since ε_i does not appear in Equation 17, we say that all charges go to the same place in energy when they hop up —the transport energy (ε_t). For typical values of $T_0 = 600\,\mathrm{K}$, $N_t = 10^{21}\,\mathrm{cm}^{-3}$, and $\gamma = \mathrm{nm}^{-1}$, the transport energy at room temperature is:

$$\varepsilon_t|_{T=300} = 0.156\ln\frac{3\left(\frac{4\pi}{3}10^{21}\right)^{1/3}}{10^7} = 0.245\,\mathrm{eV} = 4.7kT_0 \text{ and } R = 3\,\mathrm{nm}.$$

3.3.1.1. Behind the Scenes: i) Writing Equation 14 in the spirit of Mott's VRH should actually mean that R is the distance to a site in the energy band sampled by the carrier (between ε_t and ε_j) and not to a site at ε_j. Assigning each energy a unique distance required to jump across to get to it is over-stressing the effect. Namely, Equation 16 should read $\nu([\varepsilon_i, \varepsilon_j]) = \ldots$ and we should realize that the transport energy is actually a band that could be very wide (from ε_t to ε_j). ii) If we remember that we assumed carriers are at least $2kT_0$ below ε_t, then the maximum density it will hold for is: $\int_{\varepsilon_t+2kT_0}^{\infty}\rho(\varepsilon)\mathrm{d}\varepsilon = \int_{11.4kT}^{\infty}\frac{10^{21}}{2kT}\exp\left(-\frac{\varepsilon}{2kT}\right)\mathrm{d}\varepsilon = 10^{21}\exp(-5.7) \approx 3.10^{18}\,\mathrm{cm}^{-3}$. iii) The use of the exponential DOS approximation implies that the shape of the DOS at or above $\varepsilon = 0$ is not important for the transport of charges (it is not sampled by the carriers).

Using the effective energy concept to derive a conductivity value is not so simple, and naturally one has to sacrifice further accuracy to arrive at useful expressions. One such method[18] introduces two approximations:

1) The hopping rate is averaged over all sites.
2) The material is considered as a nondegenerate semiconductor, such that the Einstein relation between diffusion and mobility is constant.

The first approximation makes one loose the dependence on the actual distance between sites or the real DOS, which needs to be added manually to the formalism.[11] The second assumption is correct for exponential DOS,[20] but is not strictly valid for Gaussian DOS[21] at relatively high charge densities.

3.3.2. Percolation in Exponential DOS

In this approach, we concentrate mainly on the issue of the site density at the Fermi energy being dependent on the position of the Fermi energy (on charge density). In the context of organic semiconductors, the most relevant expression is the one derived by Vissenberg and Matters[14] and applied to amorphous-material-based transistors. For percolation approach to Gaussian DOS, see ref. [22].

Using the concept of critical conductance, the density of conducting paths (N_P) is computed by integrating over all pairs that are connected via a path with a conductivity above G_C

$$(18) N_P = \int \rho(\varepsilon_i)\rho(\varepsilon_j)H(G_{ij} - G_C)\mathrm{d}\varepsilon_i\mathrm{d}\varepsilon_j\mathrm{d}R_{ij}$$

where H is the Heaviside step function, thus allowing only for conduction paths above G_C to be accounted for. The density of sites participating in the transport is computed assuming all action occurs around the Fermi energy ($\pm\varepsilon_{Max}$):

$$(19) N_S = \int \rho(\varepsilon_i)H(|\varepsilon_i - \varepsilon_F| - \varepsilon_{Max})\mathrm{d}\varepsilon_i$$

Using the two integrals above and defining the fractional occupation of the sites as $\delta = \frac{1}{N_t}\int \rho(\varepsilon)\frac{1}{1+\exp(\frac{\varepsilon-\varepsilon_F}{kT})}\mathrm{d}\varepsilon$, the following expression for the conductivity (σ) can be derived:[14,15]

$$(20)\sigma = \sigma_0\left(\frac{\delta}{\Gamma(1-T/T_0)\Gamma(1+T/T_0)}\frac{\pi T_0^3 N_t}{\phi[2\gamma T]^3}\right)^{T_0/T}$$

where the Γ function assumes values close to 1 in the range 0.5–1.5, and ϕ is the value taken from percolation theory (Eq. 9). The result showing that the conductivity (which in many cases can be related to the concept of mobility) is dependent on the charge density through a power law is very general, and is arrived at using other models as well (when applied to similar DOS functions of course), see also Section 6.2.

3.3.2.1. Behind the Scenes: As the above method assumes that the concept of transport energy is irrelevant, it effectively assumes that the DOS is not too steep and/or the charge density is not too low.

3.3.3. Mean Medium Approximation of Gaussian DOS

The mean medium approximation (MMA) based calculation was applied to organic semiconductors and specifically to Gaussian DOS by Roichman et al.[23,24] This approach was developed in order to expand the computer-intensive theoretical treatment of localized Gaussian DOS (see discussion of Monte–Carlo simulations in Section 4) to include the notion of charge density and its effect on the transport parameters. Unlike many other models, the motivation here was more device-engineering oriented than pure physics. The idea was to find a model that could later be incorporated into semiconductor device model equations, and hence should be valid under the same assumptions (physical scenarios) as standard device models, not more nor less. While this approach does not result in analytic expressions, it does not require intensive numerical resources, and hence it is included in this section.

By mean medium it is meant that the energy distribution of states is considered to be uniform across the sample, or that each hopping site has a finite probability to be at any energy, as dictated by the DOS probability function. The initial model developed also assumed a spatially homogenous medium,[23,24] but it was later expanded to include morphological effects.[25] To include morphology, one assumes that a short-range spatial order exists, as a result of structural constrains as minimum insulating distance (for example, side chains length), molecules structure, and typical packing dimensions. The important input for a hopping transport calculation of the MMA type is the probability to find a target site at a distance R. This is conveniently described as the morphology radial correlation function, which serves as a bridge between the measurement or the model of the structure of the amorphous semiconductor and the calculation of the charge-carrier transport properties. Assuming an isotropic material without any preferred direction, the radial-correlation function is defined as:[26]

$$g(\mathbf{R_{ij}}) = g(R) = \frac{P(|\mathbf{R_{ij}}| = R)}{4\pi R^2 N_V}$$

A typical shape of a realistic site distribution and the equivalent radial distribution are given in Figure 10.

The typical radial-distribution function zeros at short distances below a minimum distance between adjacent sites (there is a minimal packing distance). In the intermediate range, there are several peaks that represent the typical distance for the (first, second) nearest neighbors (n.n.), and the long limit of the radial distribution function is a unity, as the correlation between the locations of the different sites disappears.

The calculation of the inhomogeneous MMA current for a given spatial distribution is similar to the homogenous MMA calculation,[24] where the homogenous integrand is multiplied by the radial correlation function $g(\mathbf{R_{ij}})$:

$$(21)\ \mathbf{J} = \int_{\Re}\mathrm{d}\mathbf{R_{ij}}\int_{-\infty}^{\infty}\mathrm{d}\varepsilon_i\int_{-\infty}^{\infty}\mathrm{d}\varepsilon_j g(\mathbf{R_{ij}})W_{ij}(\mathbf{R_{ij}},\varepsilon_i,\varepsilon_j - \mathbf{R_{ij}}\mathbf{E})\rho(\varepsilon_i)f(\varepsilon_i,\eta)\rho(\varepsilon_j)[1-f(\varepsilon_j,\eta)]\mathbf{R_{ij}}\widehat{\mathbf{E}}$$

Here, the integral is over all possible site distances (R), energy of initial site (ε_i), and of target site (ε_j). $g(\mathbf{R_{ij}})$ is the probability of finding a target site at distance R, $W_{ij}(\mathbf{R_{ij}},\varepsilon_i,\varepsilon_j - \mathbf{R_{ij}}\mathbf{E})$ is the hopping rate (see Eq. 2), where the term $(\varepsilon_j - g\mathbf{R_{ij}}\mathbf{E})$ accounts for the lowering of the target sites relative-energy by the electric field (E), $\rho(\varepsilon_i)$ is the DOS at energy ε_i, and $f(\varepsilon_i,\eta)$ is the Fermi Dirac occupation probability.

Using the above formalism it was possible to compute the mobility under low applied field and as a function of charge density relative to the total DOS (the DOS filling factor). Figure 11 shows the mobility computed for several Gaussian DOS widths, σ. This model indicates that in Gaussian DOS the mobility is density dependent, and that at relatively high fillings of the DOS,

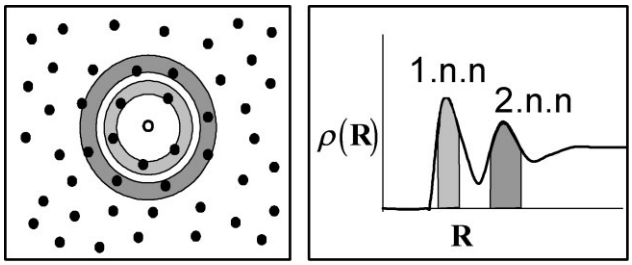

Figure 10. A schematic description of a realistic site distribution and the equivalent radial correlation function. The gray circles and the gray painted peaks present the first and second nearest neighbors location.

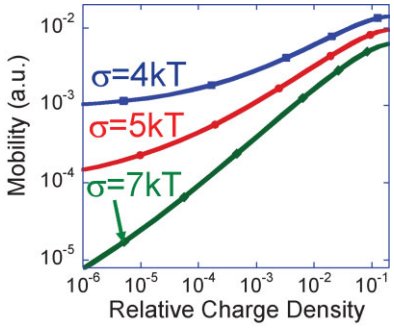

Figure 11. The low field mobility as a function of the filling of the density of states. The calculation is shown for a DOS width of 7*kT* (diamonds), 5*kT* (circles), and 4*kT* (squares).

where many devices operate, the dependence could be approximated as a power law ($\mu \propto P^{\kappa}$), with the power coefficient being:[24]

$$(22)\kappa = 0.73 - 1.17\frac{\sigma}{kT}\exp\left(-\frac{\sigma}{1.65kT}\right)$$

Figure 12 shows the electric-field dependence of the mobility calculated for two DOS widths and several charge densities. The electric-field dependence at low charge densities can be fitted to the empirical equations derived by Bassler et al.[27,28] based on Monte–Carlo simulations (see Eq. 24). However, as the charge density goes up, the electric-field dependence is significantly reduced, and the dependence on σ is suppressed as well.[24]

3.3.3.1. Behind the Scenes: i) The guiding motivation for this MMA model was to fit the physical scenario that can be reproduced by standard device models. This very practical and highly engineering oriented choice implies that physical scenarios where the notion of percolation paths is critical for reproducing the charge distribution and motion are excluded from this model (probably in the same way as such materials would be excluded from use in practical devices). ii) One of the very first assumptions of this MMA model is that the charge-carrier distribution can be described using Fermi–Dirac statistics at the lattice temperature. This implies that the high electric field regime, which causes carrier heating (see next section[11]), is excluded from this model. iii) By placing all the sites energies on the same grid, one replaces Mott's intuitive argument, which renders a deterministic link between the energy band sampled by the carrier ($\Delta\varepsilon$) and the average jump in space ($R = R(\Delta\varepsilon)$ as in Eq. 4), with the assumption that the carriers sample a significant fraction of the DOS. This implies that at low electric fields the most probable hop would be to a nearest neighbor at a distance of $\sim N^{1/3}$. As is discussed in Section 5.1, the assumption that the carriers sample a significant fraction of the DOS is in some cases equivalent to assuming that the transport is under equilibrium conditions.

4. Computer-Intensive Models for System Conductivity

Reading the preceding sections clarifies that the transport of charge carriers in amorphous organic semiconductors is modeled as hopping transport between localized states assuming specific energetic and spatial distribution functions. As we have seen, this physical framework has been studied for many years using different types of model formulations,[28–30] which differ mainly by the method used to average microscopic details to obtain a macroscopic property, such as the mobility. The Monte–Carlo approach (MC),[28,31,32] promoted by Bassler et al., is a numerical experiment performed on a finite grid of localized sites. The charges are treated as particles propagating across the grid under the influence of external field. The algorithm by which charges are propagated complies with the master equation (Eq. 1), and ensures current continuity in space is preserved (Fig. 13).

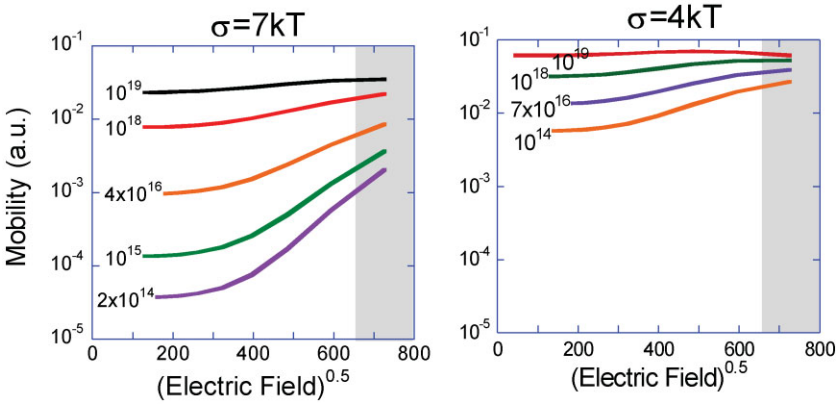

Figure 12. The calculated mobility as a function of normalized applied electric field for several charge densities at $T = 300$ K (assuming $N_V = 10^{20}$ cm^{-3}). We note that at most device operation conditions (above 10^{16} cm^{-3}) the field dependence has only little dependence of σ. The scale of the electric field was set assuming an intersite distance of 1 nm. The shaded regions denote the very high fields where carrier-heating effects (that are not included in the model) may take place.

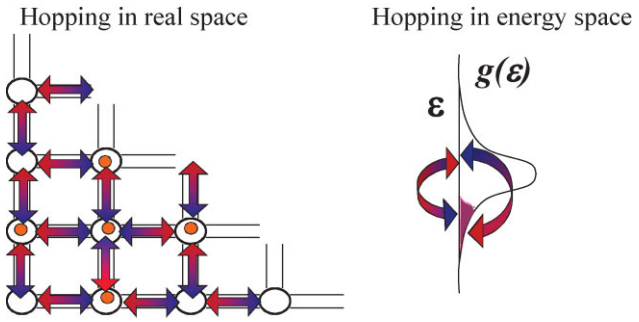

Figure 13. Schematic illustration of hopping in real space (left) and in energy space (right). The current continuity (charge preservation) is kept as a function of spatial or energetic position, respectively.

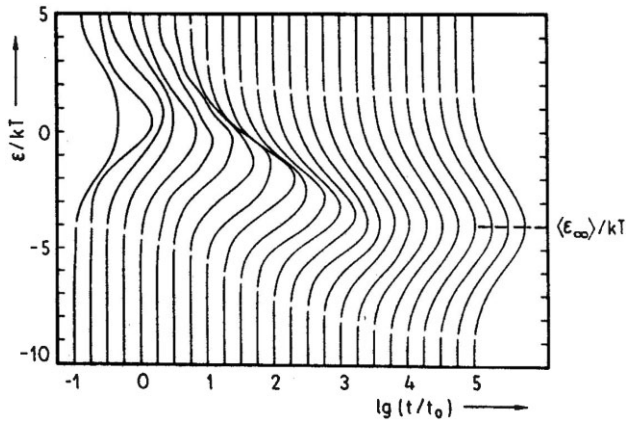

Figure 14. Example of the repetitive calculation of charge transport using MC simulation tool. The figure shows the energy relaxation of a charge packet that was (optically) injected with energy around "0" toward the steady-state distribution.[27] Note that the time scale is logarithmic, as the relaxation process, in the low density limit, is very slow and may require propagation across several micrometers.

The averaging in the MC simulations is performed by drawing different grids (sites values) and performing the calculation again until the average over the sought quantity (velocity, energy distribution, etc.) converges and the change in it becomes statistically insignificant. In the master-equation (ME) approach,[30,33] the averaging itself is performed in a very similar manner, although the basic approach of following occupation probability instead of particles renders the actual calculation different to the MC one. These two types of numerical experiments are often considered as a reference for examining other models where the averaging procedure used is not explicit (as in percolation,[13,22] effective transport energy,[18] MMA,[24] and more). A late addition to these two is the energy-space master-equation (ESME) approach[11] which is solved on a finite grid but the algorithm ensures that the current continuity is preserved in energy instead of in space (the number of charges hopping into a specific energy equals the number that are hopping out of it). We should mention that in the following we will not discuss the effect that may be introduced due to intersite interactions or other means of introducing correlation effects.[34,35] Part of the motivation for such approaches was the fact that the use of Gaussian DOS cannot reproduce all measured data,[36] and we briefly touch the issue of "real" DOS in Section 6.1.

In the most common scenario studied by the numerical models, the DOS is taking the form of a Gaussian DOS, $g(\varepsilon)$, given by:

$$g(\varepsilon) = \frac{N_V}{\sqrt{2\pi\sigma}} \exp\left(-\frac{(\varepsilon-\varepsilon_0)^2}{2\sigma^2}\right) \tag{23}$$

where N_V is the total state concentration, σ is the DOS standard deviation (width), ε and ε_0 are the energy and the center of the DOS, respectively. As ε_0 can be arbitrarily measured from any reference potential, one often sets $\varepsilon_0 \equiv 0$. As all the hops are thermally activated, most expressions derived for this DOS contain the normalized width $\overline{\sigma} \equiv \hat{\sigma} = \sigma/kT$. For example, the steady-state average energy in Figure 14 is $\varepsilon_\infty/kT = -\overline{\sigma}^2$. Figure 14 shows the time evolution of charge-energy distribution as a function of propagation time across a sample, where the calculation is of the Monte–Carlo type and is run in the low-charge-density limit. Following (optical) excitation at energies around the center of the DOS, the charge density would relax in energy until it reaches a steady state. One can see that the relaxation is taking several decades in time, which would typically correspond to propagation across several micrometers. Once steady state is established, the transport is Gaussian, and parameters such as mobility and diffusion constant can be defined and extracted.

When using an elaborate tool such as the Monte–Carlo, one can examine many physical scenarios and indeed one can acquire a great deal of intuition regarding charge transport in organic semiconductors through the large number of papers published by Bassler and coworkers (in fact, it was Ref.[37] that inspired the authors to study charge-density effects). One of the issues addresses by these studies is the effect of positional (off-diagonal) disorder, as illustrated in Figure 15a.

An example of extracting mobility value as a function of applied electric field and for different positional disorder is shown in Figure 15b. Results like in Figure 15b were used to derive an empirical relation that describes the mobility dependence on electric field and as a function of the degree of disorder.[27]

$$\begin{cases} \mu = \mu_0 \exp(-2\overline{\sigma}/3)\exp\left[C(\overline{\sigma}^2 - \sum^2)E^{1/2}\right] & \text{for } \sum > 1.5 \\ \mu = \mu_0 \exp(-2\overline{\sigma}/3)\exp\left[C(\overline{\sigma}^2 - 2.25)E^{1/2}\right] & \text{for } \sum < 1.5 \end{cases} \tag{24}$$

where $C = 3 \times 10^{-4} \mathrm{cm}^{1/2}\mathrm{V}^{-1/2}$. This equation is one of the most widely used[38] in the context of organic semiconductors, and was often used to estimate the DOS shape from transport related characteristics. At this point, it is also worth mentioning that sometimes the heuristic formula in Equation 25 is also used (Δ is the activation energy, T_0 is a characteristic temperature, B is a constant, a is the intermolecular spacing, γ is the wavefunction decay length). While Equation 25 is different from 24, both would give a similar functional form over the limited temperature range

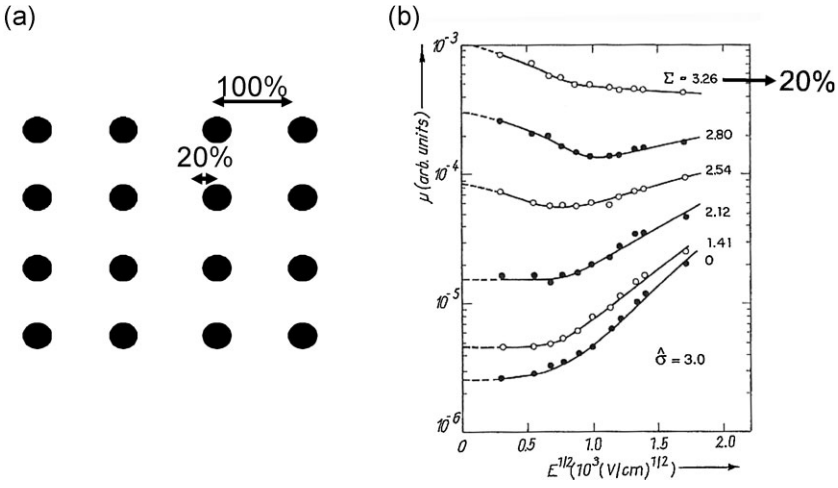

Figure 15. a) Schematic description of hopping site on a rectangular grid. The small arrow (20%) illustrates magnitude of the shift in position that may occur due to off diagonal disorder ($\sum$). b) The mobility as a function of applied electric field for several off diagonal disorder parameters. Reproduced with permission from [27].

most experiments use[39]

$$\mu(E,T) = \mu_0 \exp\left[-\frac{\Delta}{kT} + B\left(\frac{1}{kT} - \frac{1}{kT_0}\right)E^{0.5}\right];\ \mu_0 \propto a^2 \exp\left(\frac{-2a}{\gamma}\right) \quad (25)$$

The square root of the electric field in Equation 24 promotes the notion that the electric-field dependence of transport in Gaussian DOS has a Poole–Frankel nature, and thus has to do with lowering of the states in the direction of the field. This issue was recently addressed using the ESME model compared to MMA and percolation models.[11] The physical scenarios that were compared are shown in Figure 16. The top represents a case of percolation model that is solved for zero electric field, and can give information regarding only the charge-density dependence. The middle is for the MMA model, which accounts for charge-density dependence as well as the Poole–Frankel effect of lowering the site energies in the direction of the electric field. The bottom is for the ESME model, which accounts for the charge-density dependence, the Poole–Frankel effect of lowering the site energies in the direction of the electric field, and carrier heating under applied electric field.

For the comparison, we calculated the space-charge-limited current (SCLC), which is typical of organic light-emitting diode (OLED) devices. For this calculation, we first found the field- and density-dependent mobility (μ) using[24] $E = V/d$ and $P = \frac{3}{2}\left(\frac{\varepsilon V}{qd^2}\right)$. Next, we used the well-known expression[40] $J_{SCL} = \frac{9}{8}\varepsilon\mu\frac{V^2}{d^3}$. Figure 17 shows the SCLC as a function of voltage calculated for $d = 100$ nm and $\sigma = 4kT$ ($T = 300$ K). The difference between the percolation and MMA model is very small at these charge densities, implying that the barrier lowering by the electric field is not a significant factor at these densities.[24] Above 4 V (4×10^5 V cm^{-1}), the current predicted by the ESME is significantly larger compared to that of the MMA, showing that the carrier heating is the most significant factor at applied electric fields above 4–5 $\times 10^5$ V cm^{-1}. Having the above in mind, we may deduce that the most important feature missing in a percolation model is the carrier-heating phenomena, which elevates the charge distribution. This very point was only recently addressed through a modified percolation model[41] that accounts also for the electric field. However, the heating was entered into the equation not in the right place (see Eq. 26).

To understand what one means by carrier heating, we plot in Figure 18 the charge and current distribution as a function of

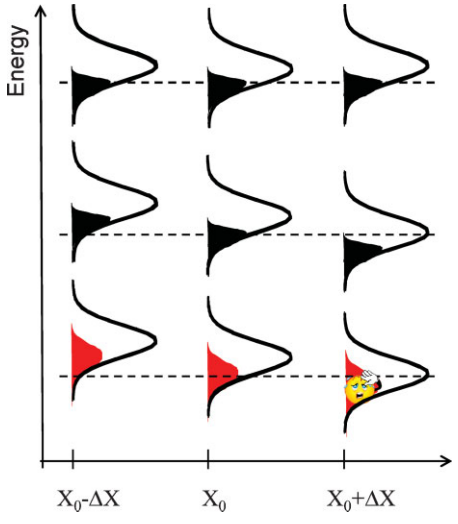

Figure 16. Illustration of three physical scenarios. From top to bottom: Percolation, MMA, and ESME.

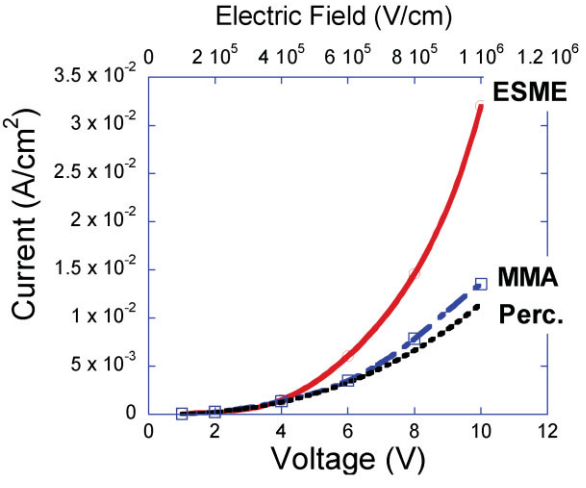

Figure 17. Calculated space-charge-limited current for a percolation model (Perc), MMA model, and ESME model. Note the importance of the carrier heating that is present only in the ESME model. In all three models, we used $a = 1$ nm, $\gamma = a/10$, $T = 300$ K, $\sigma = 4kT$, $\nu_0 = 10^{12}$ s^{-1}.

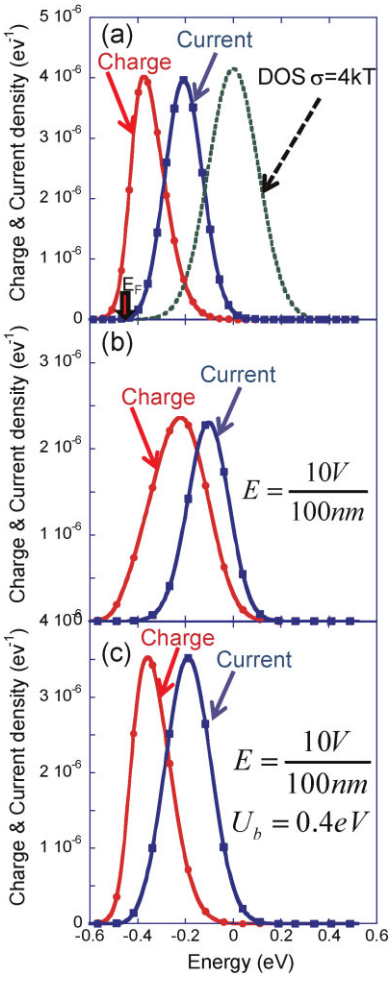

Figure 18. a) Normalized charge density, current density, and density of states for Gaussian DOS of $\sigma = 4kT$ ($T = 300$ K) under a negligible electric field. The position of the Fermi levels is marked with a thick arrow, and the filling factor of the DOS is 10^{-4}. b) Same as in a)/cm, which induces "shift upwards" of the carrier population. c) Same as in a) but for applied electric field of 10^6 V and using the polaronic rate (Eq. 3), with a polaron binding energy of $U_b = 0.4$ eV, instead of the Miller–Abraham rate (Eq. 2).

energy under several physical scenarios (calculated using the ESME model). Figure 18a was calculated under a negligibly small electric field where no carrier heating takes place. The dashed line represents the DOS distribution for a Gaussian with $\sigma = 4kT$ ($T = 300$ K), and is shown for better orientation. The charge (round symbols) and current (square symbols) distribution were calculated for a charge filling factor of 10^{-4} ($P = 10^{-4}\ N_V$). The current distribution is in arbitrara units, and was normalized to have the same height as the charge density for visual purposes.

Figure 18a shows that charges are located slightly above σ^2/kT, and that the width of their distribution is about 2/3 that of the DOS. Using the ESME, it is also possible to extract the energy of the states through which most of the current flows (square symbols in Fig. 18). Figure 18a shows that the energy band through which the transport occurs starts just above the Fermi level, and extends up to the center of the DOS' Gaussian. Figure 18b shows the same situation as Figure 18a but for an applied electric field of 10^6 V cm^{-1} (10 V/100 nm). The first thing to note is that the charge distribution shifts up and broadens in energy. It is clear that while the distribution shown in Figure 18a can be described as $p(\varepsilon) = g(\varepsilon)f(\varepsilon, T_L)$, the one in Figure 18b cannot (g is the DOS, f the Fermi Dirac function, and T_L the lattice temperature). However, if one allows the temperature used in the Fermi Dirac function to be different from the lattice temperature, it becomes possible to fit rather well the charge distribution in Figure 18b using $p(\varepsilon) = g(\varepsilon)f(\varepsilon, T_e)$ with T_e being higher than T_L. Since in order to describe the carrier distribution in energy we need to use a higher temperature, we say that the carrier distribution became hot or that carrier heating took place.

In the context of amorphous semiconductors, it was Shklovskii et al.[42,43] who originally suggested that the effect of application of electric field can be described as a rise in the effective temperature of the charge carriers. It is important to remember that the temperature of the lattice is unchanged, and in the hopping rate, Equation 2 or 3, the temperature value is the lattice temperature (carrier heating ≠ Joule heating). This may be better understood by formally writing the equation describing the net particle current flow between two sites:

$$J_{i\to j} = W_{i\to j}(T_L)f(T_e,t)_i[1 - f_j(T_e,t)] - W_{j\to i}(T_L)f_j(T_e,t)[1 - f_i(T_e,t)] \quad (26)$$

The heating of the carrier distribution is described by specifying a carrier temperature (T_e) that can be different from the lattice temperature (T_L). Therefore in the particle current, as shown in Equation 26 or even Equation 1, T_e affects only the occupation probability function (f) and not the hopping rate (W).

In Figure 18c we show, for the first time in this paper, the effect of the hopping rate being polaronic in nature (Eq. 3). The calculation is done again for an applied electric field of 10^6 V cm^{-1}, and the binding energy used for the hopping rate was $U_b = 0.4$ eV. Comparing Figure 18c to the two above it, we note that there is hardly any change in either the charge or current distribution. Namely, the polaron binding energy of 0.4 eV almost completely eliminated the carrier-heating effect. If we take this result together with what we have learned from Figure 17, then it is clear that the field dependence of the mobility would be much smaller in materials, exhibiting measurable polaron binding energy. The last thing to be learned from Figure 18 is that it shows that the charge carrier are sampling a significant fraction of the DOS, and hence we would expect that the average hopping distance would indeed be close to $N^{1/3}$ and almost independent of the width of the transport band (as it is wide enough already).

By using different material parameters, it was observed[11] that the fitting parameters T_{eff} and E_f depend on the field strength (normalized by the distance between sites) and the phononic temperature of the media. However, in agreement with the general prediction in Ref. [42], T_{eff} and E_f are independent of the charge-carrier concentration and the disorder parameter, be it σ for Gaussian disorder or E_0 for exponential DOS. The effective temperature dependence on the applied electric field for a fixed lattice (phonon) temperature is shown in Figure 19. The circles denote the carrier temperature in exponential DOS and the squares for Gaussian DOS. The solid lines are fits using the

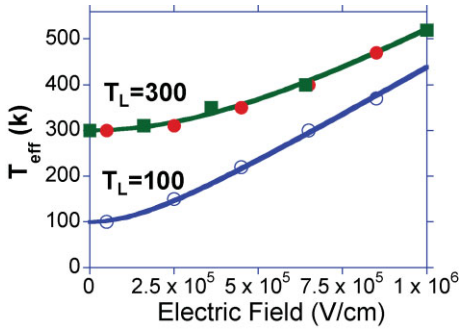

Figure 19. Effective temperature of the carrier population in Gaussian (squares) and exponential (circle) DOS as a function of applied electric field ($a = 1$ nm). The solid line is the heuristic formula: $(T_{\mathrm{Eff}}/T_{\mathrm{L}})^2 = 1 + [0.37Ea/(kT/q)]^2$.[43] Higher curves were calculated for lattice temperature of 300 K, and the lower for 100 K.

dependence suggested in Ref. [43]:

$$(T_{\mathrm{Eff}}/T_{\mathrm{L}})^2 = 1 + [mEa/(kT/q)]^2 \tag{27}$$

We note that the original work[42] predicted the factor m to be 0.5, and our fit results in 0.37 ± 0.02.

The other issue that was examined in Ref. [11] with respect to the carrier-heating phenomena is the hopping rate. Figure 20 shows the effective temperature as a function of applied electric field for the Miller–Abraham rate and for the polaronic rate. It is clear that the amount of heating, or the numerical factor in Equation 27, is dependent on the functional form of the hopping rate, and that for larger polaron-binding energy the heating phenomena is almost entirely suppressed. This can be at least partially understood with the aid of Figure 4, which shows that as the polaron binding energy increases the hopping is more directed towards lower energies. Hopping that is preferentially to

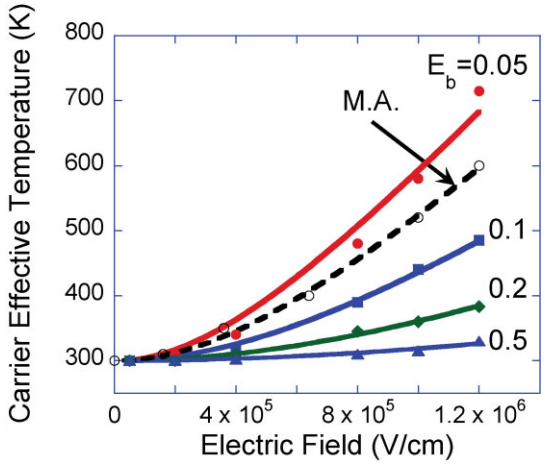

Figure 20. Effective carrier temperature for lattice temperature (T_{L}) of 300 K and varying polaron binding energies. Also shown in a dashed line is the result of the calculation using the Miller–Abraham's rate. The solid lines are fits using the heuristic formula: $(T_{\mathrm{Eff}}/T_{\mathrm{L}})^2 = 1 + [mEa/(kT/q)]^2$, where m varies between 0.45, for $E_{\mathrm{b}} = 0.05$ eV, and 0.1, for $E_{\mathrm{b}} = 0.5$ eV.

significantly lower energies acts against the field that "tries" to push the carriers upward.

5. Non-Averaging Approach

Sometimes one has to admit that averaging over many events to arrive at a mean value is not meaningful, since the spread of values (or standard deviation) could be as large or larger than the quantity in question. In such cases, one would often use the phrase "dispersion" to indicate the wide spread of values. In the context of charge mobility, this was first addressed by Scher and Montroll,[29,44] which stated in their abstract "...the theory shows the limitations of the concept of a mobility in this dispersive type of transport." In their work, the physical picture that arises is that in a disordered material some of the states act as deep traps, and if the energy distribution takes longer than the measurement-time window to reach equilibrium (infinite time on the measurement timescale), the charge velocity would be time dependent, and hence the concept of mobility would be hard to implement. It was also shown that if the measurement window is made wide enough, the transport would eventually become nondispersive.[45] In Figure 14 one could expect the transport to become nondispersive only after about four decades in time.

As the relevant film thickness of organic semiconductors shrank from the micrometers used in the xerography days to ~100 nm in the OLED days, an alternative view of dispersive transport was suggested.[46,47] Instead of suggesting that the charge-energy distribution is a function of time, it was argued that for thin films the energy distribution of the charges is different across the plane of the film, and hence is a function of xy spatial coordinate. If the theory by Scher and Montroll led us to the notion that to reach equilibrium one needs to let the measurement span a long enough time window, or that the film needs to be thick enough, now Rappaport suggests that the film width is a critical factor as well. This brings us to a somewhat philosophical question of the actual meaning of "equilibrium" in disordered molecular semiconductors.

5.1. Equilibrium in Molecular Semiconductors

When we decided that the molecular semiconductors we address here are those whose states are localized, we also assumed that once a charge hops onto a state (molecule), it loses all its excess energy and becomes at equilibrium with the molecule (state). So what does "equilibrium" mean in the context of charge transport across many sites? To avoid deep philosophical questions, we only check our formalism as to where this issue of equilibrium is being used. In the context of charge transport in devices, one can safely state that equilibrium enters only to justify the use of Fermi–Dirac statistics in describing the charge distribution in energy. Namely, it is used to justify Equation 28, and typically one only requires that its integral form, Equation 29, holds to a good approximation.

$$p(\varepsilon) = g(\varepsilon)f(\varepsilon, T) = \frac{g(\varepsilon)}{1 + \exp\left(\frac{\varepsilon - \varepsilon_{\mathrm{F}}}{kT}\right)} \tag{28}$$

$$P = \int p(\varepsilon)\mathrm{d}\varepsilon = \int \frac{g(\varepsilon)}{1+\exp\left(\frac{\varepsilon-\varepsilon_F}{kT}\right)}\mathrm{d}\varepsilon \quad (29)$$

In the above equations, only the DOS (g) is material or device/processing-dependent, hence we are led to examine its role or origin. In the previous Sections 3 and 4, we assumed the sample to be infinite, and by DOS we meant that it could reproduce the imaginary experiment in which we map all the states in the infinite sample and create a histogram showing the number (density) of states per energy interval.

In order for the sample to be considered infinite, two conditions must be fulfilled: i) the sample should be large enough so that the histogram of the states' energy is independent of its size, and ii) every charge has sampled a significant fraction of the sample (the charges "know" that the sample is infinite). Figure 21 illustrates point i), where Figure 21b and c show the energetic surface created by 400 sites, the energies of which were drawn randomly from the Gaussian DOS shown as a solid line in Figure 21a. The contour (Fig. 21b) and surface (Fig. 21c) show the typical roughness of the energy surface of disordered semiconductors. The dashed line in Figure 21a shows the histogram of the 400 states, which looks relatively close to the original DOS shown in the solid line. However, it should be clear that if the fit is only close to being good at the center of the Gaussian, it would be far from being reasonable at the tails (remember that low-density carriers reside at $-\sigma^2/kT$). So the idea of the sample having to be large enough such that the actual DOS would resemble the "theoretical" DOS becomes relatively obvious with the aid of Figure 21. However, the notion that every charge has to sample a significant fraction may be less obvious as one needs to put him/herself in place of the electron and imagine what it "sees."

To address this "seeing through the eyes of the charges", we examine Figure 22. Figure 22a and b describes essentially the same sample, but in Figure 22a the charges propagate along the long axis, while in Figure 22b it is propagating along its short axis of the sample. In this figure, the sites are described as circles, and the filling fraction of each circle corresponds to its energy.

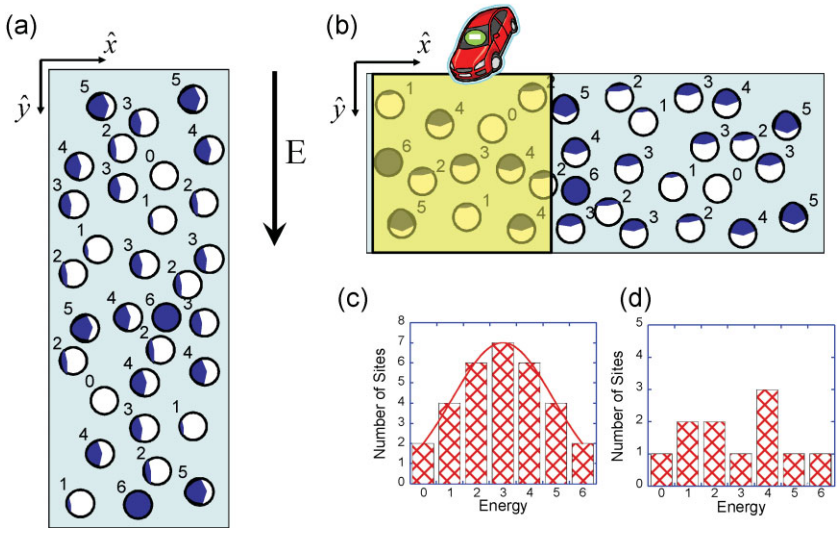

Figure 22. a) Schematic description of a sample made of discrete hopping sites. Sites are described as circles, and the filling fraction of each circle corresponds to its energy. b) Schematic description of the same sample but with different orientation with respect to the electric field. The square area illustrates the volume sampled by a drifting carrier. c) DOS of the samples shown in a) and b). d) DOS experienced by a charge sampling the square area in b).

Figure 22c shows the histogram of the sites energies for the samples in Figure 22a and b, which is similar to the central region of a Gaussian (shown in solid line). Now we place ourselves in the eyes of an electron, and try to visualize what it sees as it travels across the sample. If we send a charge across the sample, we would expect it to sample a region having an area (volume) that is proportional to the propagation length. The yellowish (shadowed in B&W) square on the left side of sample b exemplifies such a sampled region, and Figure 22d shows the histogram of the sites energy in that region.

The distribution in Figure 22d is so different to the one in Figure 22c that we can safely say that if Figure 22c describes the DOS function (g), then neither Equation 28 nor 29 could be satisfied in this sampled region. This leads us to one of two conclusions: i) charges moving across a thin sample can never be at equilibrium; or ii) the Gaussian DOS is not appropriate to describe the transport, and a more "local" version should be used (as in Fig. 22d). It is also clear that if we move the yellowish square to the right, we will produce different shapes for the local DOS, or in other words, charges starting at different positions would cross the sample under a different time with a different velocity. Namely, there is a variation or dispersion of the velocity that could be interpreted as dispersion in the mobility, and in this case it is a spatial dispersion.[46,47]

Turning to the long sample depicted in Figure 22a, we can imagine the same yellowish square expanding across it as a function of time. Namely, the local DOS or the sampled DOS would gradually change from Figure 22d to c. This tells us that the velocity of charges is going to be time dependent, or that there is a time-domain dispersion of the mobility.[29,44]

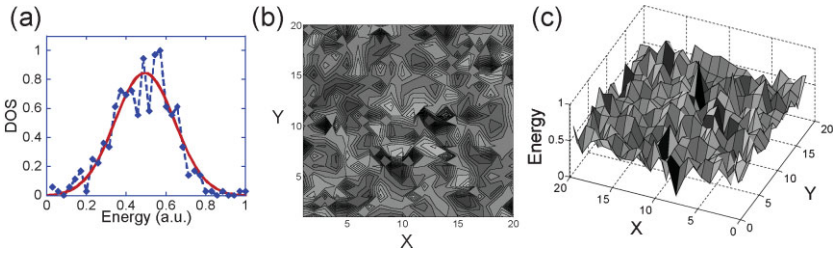

Figure 21. a) Hypothetical Gaussian DOS (solid line) and the histogram of 400 states (dashed line) drawn based on this Gaussian probability. b) Contour map of the 400 states (sites) drawn. c) 3D surface map of the 400 states (sites) drawn.

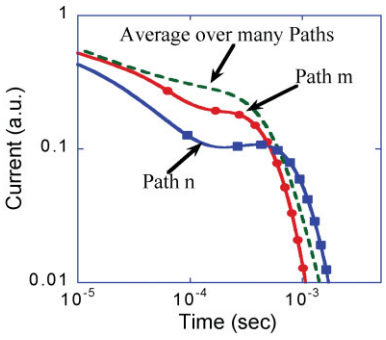

Figure 23. Time-resolved current transient as a result of an impulse charge excitation at $x = t = 0$ (simulation of classical time of flight). The round and square symbols are single-run results (specific paths), and the dashed line is an average over many such runs. The sample length is 75 nm.

This also helps us understand why if we take a sample big enough and let the charges propagate for a long enough time they will eventually reach equilibrium and the transport would stop being dispersive (see Fig. 14 and Ref.[45]). This also suggests that for thin (disordered)-film devices, where the charge-propagation time is by definition very short, the dispersive transport would constitute an almost intrinsic property.

To test the idea of the above non-averaging approach, a numerical simulation based on the master-equation approach was conducted.[47] To be consistent with published literature, the numerical simulation was of a time of flight experiment, and the numerical experiment used a sample with dimensions of 9 nm × 9 nm × 75 nm. The infinite-size sample was assumed to be relatively ordered, characterized by a Gaussian energy distribution having standard deviation of $\sigma = 3kT$. The typical procedure for calculating the TOF response would be to draw different samples (paths) until the average result becomes independent of the number of draws made. Such a procedure resulted in the dashed line in Figure 23, illustrating that for the thin, 75 nm, film simulated, the transport is highly dispersive. However, the individual paths, denoted by round and square symbols, exhibit a distinct plateau over a significant fraction of the propagation time. Namely, the local transport, which is associated with the local DOS, is not dispersive. From such a numerical experiment one can conclude that the dispersive nature of thin samples is largely due to spatial non-uniformities occurring on the nanometer (10 nm) scale.

5.2. Spatially Dispersive Transport or Mobility Distribution Function

Based on the above discussion, we can say that spatially dispersive transport allows sample to be viewed as if it was divided into subunits or pathways (Fig. 24), each characterized by its local DOS and consequently by a typical charge velocity or mobility. The volume of this imaginary pathway would be roughly the volume that a charge would sample as it drifts and diffuses towards the opposite contact.

If one excites the sample by generating electrons at the contact boundary using a step-function temporal shape, then at different places charges would propagate at different speeds (see schematic

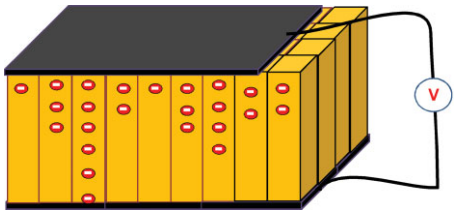

Figure 24. Illustration of spatial distribution of current paths (mobility values) in a thin-film device. The minus signs illustrate the response to a step function charge injection at the top electrode.

description in Fig. 24). The current flowing through the sample can then be mathematically described as:[46]

$$J_e(t) = APq\left\{\int_{\frac{d^2}{Vt}}^{\infty} g(\mu_e)\mathrm{d}\mu_e + \int_0^{\frac{d^2}{Vt}} g(\mu_e)\frac{t}{t_{tr}(\mu_e)}\mathrm{d}\mu_e\right\} \quad (30)$$

where J_e is the electron current density, $g(\mu_e)$ is the mobility distribution function (MDF) for the electron pathways, $t_{tr}(\mu_e)$ is the transit time across the device for an electron with mobility $\mu_e\left(t_{tr}(\mu_e) = \frac{d^2}{\mu_e V}\right)$, d is the device thickness, q is the electron charge, P is the incident light intensity, and A is the carrier pair generation efficiency (number of electron-hole pairs generated per unit of incident intensity). The first term in the brackets represents the pathways that have reached their steady state by time t (have a mobility value higher than $\frac{d^2}{tV}$). The second term represents paths with lower mobility, which have not reached steady state by time t. Equation 30 can be manipulated to form an analytic expression for deriving the MDF:[46]

$$g(\mu) = g\left(\frac{d^2}{Vt}\right) = -\frac{d^2 I(t)}{\mathrm{d}t^2}\frac{2Vt^3}{APqd^2} \quad (31)$$

We note that the above derivation assumed that for each path the mobility can be defined and that temporal dispersion effects are not significant. In cases where the disorder is large and the spatial distribution is also mixed with significant temporal dispersion, the MDF described above should read velocity distribution function.

6. Implications and Uses for Device Analysis

6.1. The Density of States Function

As we have seen in the previous sections, there are different models one may use for device analysis, and the preferred choice may depend on the shape of the DOS. Hulea et al.[48] were probably the first to attempt a direct measurement of the electronic DOS in semiconducting-molecule/polymer-based films. Using electrochemical doping of OC1C10-PPV, they found that the DOS was essentially exponential, and that only at very high densities (above 0.5 per monomer), which are probably

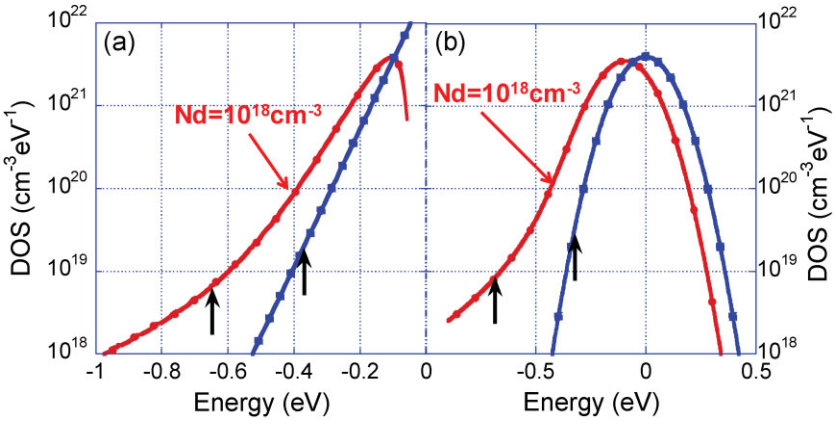

Figure 25. Density of states as a function of energy. a) The bottom curve (square symbols) shows undoped exponential DOS ($T_0 = 600$ K, $N_t = 10^{21}$ cm^{-3}), and the top one (round symbols) shows the case of adding ionized dopants at a density of 10^{18} cm^{-3}. b) The bottom curve (square symbols) shows undoped Gaussian DOS ($\sigma = 0.1$ eV, $N_V = 10^{21}$ cm^{-3}) and the top one (round symbols) shows the case of adding ionized dopants at a density of 10^{18} cm^{-3}. The vertical lines show the position of the Fermi level for a charge density of 10^{18} cm^{-3}.

above any practical device-operating conditions, the DOS can be somewhat fitted to a Gaussian DOS. The only reservation with respect to a measurement performed through electrochemical doping is that dopants tend to alter the DOS.[49,50] Figure 25 shows the effect of doping on both exponential and Gaussian DOS calculated using the formalism described in Refs.[49,50]. One can observe in Figure 25 that the transition from the dopant-induced exponential-like tail of the main DOS function occurs at a DOS value that is 10 times the doping level. We should also mention that exponential-like tails are a general phenomena associated with random distribution of scattering potentials.[51]

Tal et al.[52] have developed a technique based on the use of Kelvin-probe measurements of the channel in a FET as a function of gate bias. Data similar to the one published in Ref.[52] is shown in Figure 26, and it indicates that the DOS of an undoped α-NPD is Gaussian with an exponential tail. It also shows that by doping to a level of 10^{18} cm^{-3}, the DOS broadens, and that the deviation from a Gaussian occurs at a DOS value that is about 10 times higher (in agreement with the observation made on Fig. 25). Having this in mind, we return to the undoped DOS (solid line in Fig. 26), and it seems now that we should refer to the undoped

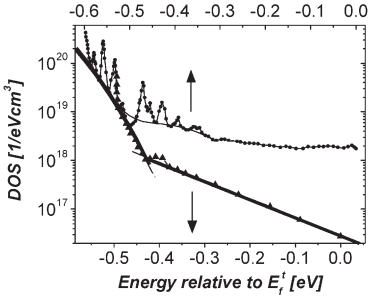

Figure 26. DOS versus energy relative to E_f^t (E_f at $V_{GS} = V_t$) for undoped (solid triangles) and doped (solid circles) samples. The solid curves are fitting of a Gaussian function and an exponential tail to the undoped sample DOS.[52]

sample as non-intentionally doped to a level of $\sim 10^{17}$ cm^{-3}. However, the FET characteristics showed an ON ($V_{GS} = -7V$) to OFF ($V_{GS} = 0V$) ratio of 10^6,[53] which immediately rules out such high level of doping. It is tempting to conclude that the exponential tail is an intrinsic bulk phenomenon, but one has to remember that the measurement was done on a very thin TFT channel that was in close proximity with the dielectric interface. Veres et al.[54] argued that the gate dielectric may induce broadening of the DOS due to potential fluctuations associated with internal dipoles,[55] and we may add that the low density of trapped charges at the insulator would have a similar effect.

To conclude this section, we can only say that the DOS in organic semiconductors is probably a combination of a Gaussian and an exponential DOS, where the relative contribution of each may depend on the purity of the film and the device it is embedded in. For example, the discussion above indicates that the role of the insulator in organic TFTs is to enhance the contribution of exponential-like tails, and that it would be reasonable to assume that in some cases it may obscure any ''intrinsic'' DOS.

6.1.1. Generalized Einstein Relation

A property that is closely related to the shape of the DOS is the Einstein relation. One way of deriving the Einstein relation starts from the continuity equation $J_h = \mu_h n_h E - D_h \frac{d}{dx} n_h$, and assumes that the total current is very small compared to the drift and diffusion currents ($J_h \ll \mu_h n_h E$; $D_h(d/dx)n_h$), such that one can neglect it and write $\mu_h = D_h \frac{1}{n_h}\frac{dn_h}{Edx} = -D_h \frac{1}{n_h}\frac{dn_h}{dV}$. The last step is assuming equilibrium such that the voltage drop can be replaced with the difference in Fermi level, and we arrive at $\mu_h = -D_h \frac{1}{n_h}\frac{dn_h}{dE_f} = -D_h \frac{1}{n_h}\frac{d}{dE_f}\left[\int \frac{g(\varepsilon)}{1+\exp\left(\frac{\varepsilon-\varepsilon_F}{kT}\right)} d\varepsilon\right] \triangleq D_h \frac{q}{kT}\frac{1}{\eta_D}$.[1] Knowing the states density as a function of energy (DOS) allows calculating the Einstein relation as a function of the position of the Fermi level energy (charge density) relative to the DOS and vice versa.[21,56] An example of such calculation is shown in Figure 27, which uses Gaussian DOS of different widths and with $N_V = 10^{20}$ cm^{-3}.

The fact that the enhancement of the Einstein relation (η_D) actually tracks the DOS function is depicted in Figure 28 for a Gaussian DOS with $\sigma = 4kT$ ($T = 300$ K). The fraction of the DOS filled by the charge carrier as a function of the Fermi level is shown in round symbols. The dotted line shows a dependence of $\exp(-\Delta E/kT)$. We note that at charge densities above 10^{-5} of the total DOS the charge-density dependence becomes less sensitive to changes in the Fermi level. Examining Figure 27 we note that this is exactly the energy at which the enhancement of the Einstein relation (η_D) starts to grow. Also shown in Figure 28 is the DOS function (square symbols).

6.2. Analyzing Disordered Organic TFTs

Effectively, most of the analysis applied to disordered organic materials is relying on them being disordered and not so much on

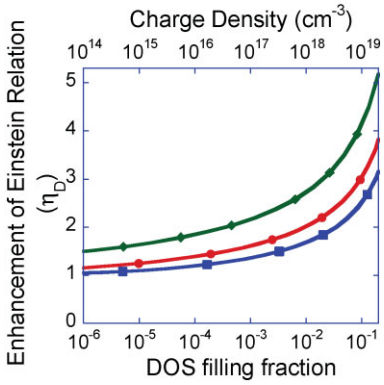

Figure 27. Enhancement of the Einstein relation, relative to the low-density limit (kT/q), as a function of the filling of the density of states.

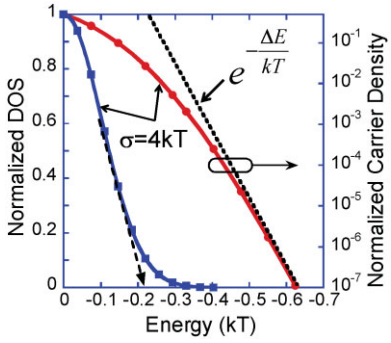

Figure 28. DOS (square symbols, left axis) as a function of energy and the charge density as a function of the Fermi-level energy (round symbols, right axis). The arrow indicates the onset of the DOS as would be determined in cyclic voltammetery methods. The dashed line shows the slope of a Boltzmann factor. Note that at charge densities above 10^{-5}–10^{-4} of the total density of sites the charge density becomes less sensitive to changes in the Fermi-level position.

them being organic molecules. In that context, one should also mention the vast literature developed for amorphous silicon (a-Si)-based TFTs.[57,58] In the field of a-Si, it is well accepted that the transport is affected by deep exponential-like trap states, and in the context of field effect transistors one uses the power law dependence of the mobility:[59,60]

$$\mu = \mu_0 \left(\frac{V_{GS} - V_T}{V_{AA}} \right)^{\gamma} \tag{32}$$

or a channel-conductance formula of:

$$g_{ch} = \frac{W}{L} C_i \mu_0 \frac{1}{V_{AA}^{\gamma}} (V_{GS} - V_T)^{1+\gamma} \tag{33}$$

And if we use the fact that the channel width is to a good approximation proportional to $(V_{GS} - V_T)^{-1}$, then the 3D charge density (δ) at the channel is proportional to $(V_{GS} - V_T)^{-2}$. Using Equation 32, we find:

$$\mu = \frac{\mu_0}{\delta_{AA}^{\gamma/2}} \delta^{\gamma/2} \tag{34}$$

If we substitute $\gamma/2$ with T_0/T or κ, then Equation 34 becomes similar to Equation 20 derived by Vissenberg and Matters[14] for transport *within* an exponential DOS (see Section 3.3.2), or Equation 22 derived by Roichman et al.[24] for transport *within* Gaussian DOS (see Section 3.3.3). Analysis of TFTs based on the assumption that the mobility is governed by a power law is abundant in the a-Si literature, and is also used in the field of organic semiconductors.[14,61]

There are several things to note while analyzing TFTs that are based on a material exhibiting charge-density dependence of the mobility.

Using the known formula $\mu = \frac{L}{WC_iV_{DS}} \frac{\partial I_{DS}}{\partial V_{GS}}$ carries the hidden assumption that $\frac{\partial \mu}{\partial V_{GS}} = 0$.

There is also a field dependence of the mobility, plus at high V_{DS} values the charge density across the channel is not uniform. Extracting at low drain-source voltages helps to overcome these problems.

In this context, it is worth mentioning the device analysis presented in Ref.[62], which showed that by careful design and measurement procedures it is possible to extract both charge density and electric-field dependence of the mobility. In this paper, they used the model by Roichman et al.[24] or its concepts, which account also for electric-field dependence, to explain the physical picture.

6.2.1. Channel depth and the Einstein Relation

It is possible to show that the channel depth ($X_{Channel}$) can be approximated[24] as

$$X_{Channel} \approx \frac{d_{ins}}{V_G - V(\gamma)} \frac{\varepsilon_\pi}{\varepsilon_{ins}} \frac{kT}{q} \eta \tag{35}$$

Here d_{ins} and ε_{ins} are the thickness and dielectric constant of the insulator, respectively. E_p is the dielectric constant of the organic semiconductor, $V(\gamma)$ is the potential at the channel ($V_{Source} \leq V(\gamma) \leq V_{Drain}$), and η is the Einstein enhancement factor, which is charge-density dependent (see Fig. 27). Examining Equation 35 it seems that by applying high gate bias the channel depth would shrink towards zero and consequently the charge density at the channel would increase with no limit. This is of course not physical, since the maximum charge density cannot exceed the total DOS (N_V). This is where η becomes very important, and one can consider that, in the current context, η would increase so as to enhance the channel depth and prevent the charge density from exceeding that of the DOS. Figure 29 shows the calculation of the channel depth (round symbols) and the charge density (square symbols) as a function of gate bias. At first the channel depth does vary almost like $1/V_G$, but then it flattens at about 1 nm, and above 14 V it starts slowly to increase. Accordingly, the charge density rises steeply at low gate bias, and then only asymptotically approaches the total DOS

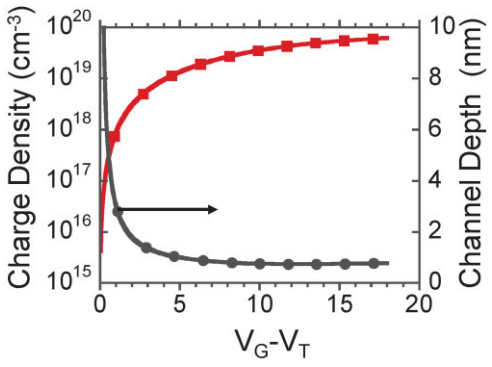

Figure 29. Calculated charge density and channel depth as a function of gate bias for a disordered conjugated material. The calculated is for $\sigma = 7kT$ and $N_V = 10^{20}\,cm^{-3}$.

($N_V = 10^{20}\,cm^{-3}$) as the increase in η prevents it from reaching N_V.

6.3. Analyzing Disordered Organic LEDs

In organic LEDs, we are typically concerned not only with transport within the layer but also in charge transport to a disordered media, charge transport between two layers, and charge recombination, which is also transport limited.

6.3.1. Transport and Mobility

Regarding the transport itself, we can use Figure 17 to help us decide which mechanism is most relevant for devices that are not contact-limited. We can see that up to about 4 or 5 V (across ~100 nm) the charge-density dependence of the mobility is the governing factor, and above 5 V it is the field dependence (via carrier heating) of the mobility that is governing the *I–V* curve. Also, if the device has non-ideal contacts, then the charge density within the device would not rise as much as a function of applied voltage, and hence the range where the field dependence is important will extend to lower voltages. This helps us rationalize why using the model promoted by Bassler et al. (see Section 4 and Eq. 24) was so successful in describing and analyzing the properties of organic LEDs despite the fact that it does not account for charge-density effects.

6.3.2. Charge Injection

Injection into amorphous semiconductors can be analyzed by considering: i) fluctuation of injection barrier heights,[63,64] ii) hopping rates from a metal into a disordered (Gaussian) DOS,[65,66] iii) analyze the transport across the image potential as overcoming the surface recombination rate at the contact, and[67,68] iv) charge transport across the image-force related barrier assuming equilibrium conditions and accounting for the DOS.[69] The advantage of the 4th approach is that it relies on standard device model equations, where the effect of the DOS shape can be entered through the generalized Einstein relation (see Fig. 30).

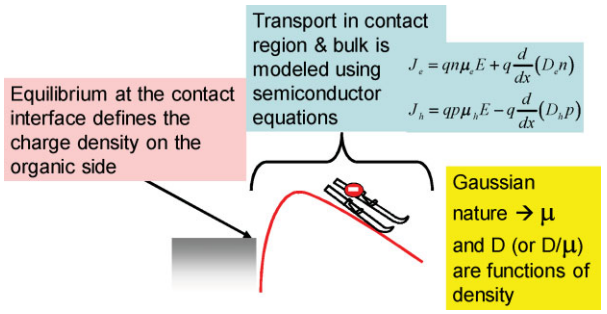

Figure 30. Schematic description of the mechanisms governing charge transport across the metal-organic semiconductor interface.

We should remember that the macroscopic semiconductor device model is generally applied to thermalized carriers only, and hence if one wants to include the contact region in such a model, the thermalization length must be negligibly small. The issue of thermalization length of carriers in the context of charge injection is described in ref. [67], which treats the injection using one dimensional Onsager theory. From this paper, we only quote here the approximate expression for the thermalization distance for hot carriers, $x_t \approx \mu v_0 (m/e)$, where $\mathbf{v}_0$ is the initial velocity of the injected carrier, μ is the mobility, and m is the carrier mass. This equation illustrates the relevance of the low-mobility to the physical picture. Although the mass of a carrier-polaron is not well known, the overall thermalization length is believed to be in the range of 1–0.1 nm, and hence one may assume that the carriers thermalize at first-hop site,[65] and that any further motion of the carrier is governed by hopping transport in the electronic potential.

Using the 4th approach, it is possible to show that many of the unique features or "anomalies" in contact phenomena can be traced back to the simple fact that in a Gaussian DOS the change in charge density due to a change in Fermi level (contact workfunction) does not follow the rule of $\exp(-\Delta E/kT)$[69] (see Fig. 28). Detailed experimental studies, however, have shown that such an approach on its own is not sufficient,[24] and that one should probably also allow for a modified DOS close to the contact interface.[70,71] This observation along with the discussion in Section 6.1 strengthens the general statement that the DOS at the interface, be it metal or insulator, is very likely to be different from the bulk one, and could impact measurable device properties. Despite the importance of the details of the DOS at the interface as a rule of thumb, one can state that a contact barrier of up to about 0.4 eV is not likely to limit the current in the device at room temperatures.

6.3.3. Charge Transport Across Layers

On the semiconductor device model level, the transport in the device is governed by[72]

$$\frac{\partial}{\partial t} n_e(z,t) = \frac{\partial}{\partial z}\left[D_e \frac{\partial}{\partial z} n_e(z,t) + \mu_e(E) n_e(z,t) E(z,t) \right] - R_e(z,t) n_e(z,t) \quad (36)$$

At the interface between two materials, one would expect a discontinuity that would affect the result of the $\partial/\partial z$ on the right-hand side. In organic semiconductors, the mobility values vary by orders of magnitudes between different materials,[73] and the electric-field dependence of it also varies between materials. This has led to the notion of mobility barrier, which could be significant.[74,75] The other, more common, effect is that under quasi-equilibrium conditions a difference in the energy levels should result in a difference in the charge densities on both sides of the interface, which in the case of Gaussian DOS could be formally written as:

$$\begin{cases} N_1 = \int \frac{N_{V1}}{\sqrt{2\pi}\sigma_1} \exp\left(-\frac{(\varepsilon-\varepsilon_{01})^2}{2\sigma_1^2}\right) \frac{1}{1+\exp\left(\frac{\varepsilon-\varepsilon_F}{kT_e}\right)} d\varepsilon \\ N_2 = \int \frac{N_{V2}}{\sqrt{2\pi}\sigma_2} \exp\left(-\frac{(\varepsilon-\varepsilon_{02})^2}{2\sigma_2^2}\right) \frac{1}{1+\exp\left(\frac{\varepsilon-\varepsilon_F}{kT_e}\right)} d\varepsilon \end{cases}$$

As Figure 28 shows, a change in the relative position of the Fermi level with respect to the DOS ($\varepsilon_0 - \varepsilon_F$) will result in a change in the equilibrium charge density. The other parameters that are less obvious are the actual density of sites (N_V), that could vary as a function of the molecular structure, and especially when molecular blends are used, and the disorder (σ). A careful reader would notice that in the expression for the Fermi function we wrote T_e. This implies that carrier heating will diminish the effect of the energy difference that is weighed by the temperature describing the charge-energy distribution.

6.3.4. Charge Recombination & Light Emission

Charge recombination in organic LEDs is considered to be a diffusion-limited process or Langevin recombination process. The recombination is by nature a bimolecular process with a rate of the form $R_{REC} = BNP$. The pre-factor B is calculated for a process in which the charges are being attracted by their mutual electric field:

$$B = \frac{q}{\varepsilon_0\varepsilon_r}(\mu_e + \mu_h) \stackrel{?}{=} \frac{q}{\varepsilon_0\varepsilon_r}(\mu_e(E) + \mu_h(E)) \quad (37)$$

As discussed in previous sections, the mobility is dependent on the applied electric field. Can we expect the applied-electric-field effect on the mobility to be relevant for the recombination rate of two charges that are randomly positioned with respect to each other? If we consider only the Poole–Frankel-type effect of lowering the barriers in the direction of the field, then the answer would probably be "no" or "very slightly." The reasoning is that the field induced lowering of the barriers is occurring over a very limited solid angle out of the full sphere describing the motion direction of randomly positioned pairs. If we consider the mechanism of carrier heating, where carriers are being elevated in energy, then the answer would be a definite yes. The reasoning here is that the higher position in energy is not-directional (in space), and hence the mobility is enhanced not only in the direction of the electric field. Again, Figure 17 tells us that above ~5 V the main contribution is due to carrier heating, and hence at voltage above 5 V one should definitely use field-dependent mobility in the recombination rate. In Ref. [76] this question was addressed experimentally, with both the light output and charge density measured simultaneously in response to a square wave pulse of about 30 V (see Fig. 31). Examining the turn-off dynamics, we note that at short times there is no correlation between the light and charge density inside the device, and that at longer times they follow almost the same time dependence. If the instantaneous drop in electroluminescence is not due to lowering of the charge density, then we are left only with the recombination pre-factor B that could be changing (turning off) as the applied voltage (electric field) is removed. Namely, at high applied voltages the recombination prefactor must be written using field-dependent mobility, and in Ref. [77] it is shown to be important already at 5 V (across 75 nm). If one accepts that the recombination depends on the electric field in the same manner as the mobility is, it then becomes possible to monitor time evolution of the electric field inside the device through recombination (light output) dynamics.[77]

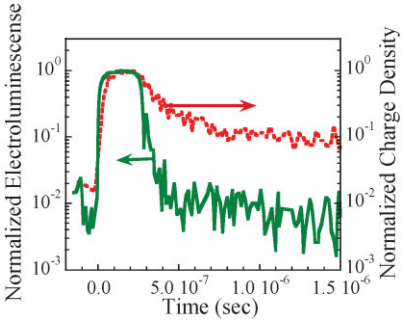

Figure 31. Measured light and charge density in a poly(p-phenylene vinylene) (PPV) LED in response to a short square pulse of 27 V.

6.4. Spatial Non-Uniformities

There could be many types of non-uniformities in devices, especially where contacts are involved or materials are being adjoined. The most obvious sources are adhesion of metal layers, nonflat substrates (as spikes in non-ideal indium tin oxide (ITO) layers), the conductivity fluctuation across conducting polymers (as poly(3,4-ethylenedioxythiophene) (PEDOT)), and partial crystallization.[78,79] To these, we have added, in Section 5.2, the spatial distribution of the mobility, which arises from the disordered nature of most light-emitting materials. While it is not obvious if and what can be done to completely eliminate all the spatial non-uniformity, it is possible to post-characterize it and use screening procedures to minimize the effect. Such could be based on scanning probe techniques[80] or through the analysis of device properties under step-function excitation conditions (see Fig. 32).[81]

It was suggested[81] that such non-uniformities affect the device lifetime, and that this is part of the reason for green-PPV based devices having longer lifetimes. The other effect of any of the above-discussed non-uniformity types is related to the reduction in charge recombination and the consequent reduction in light-emission efficiency. The reasoning is that any non-uniformity is not likely to affect both electrons and holes in the

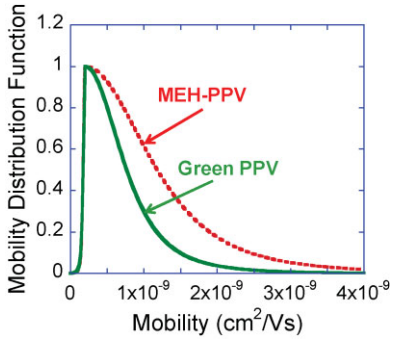

Figure 32. The mobility distribution function measured for two thin-layer devices based on different light-emitting polymers: poly[2-methoxy-5-(2'-ethyl-hexyloxy)-1,4-phenylene vinylene] (MEH-PPV) and Green-PPV (structure details can be found in Ref. [81]).

exact same manner. Hence, it would induce spatial separation, that would lower the device efficiency.[82]

6.5. "Extrinsic" heating

It is unthinkable to discuss the basic physics of organic LEDs without touching a very critical factor such as joule heating. As organic LEDs are typically built on glass substrates, the heat dissipation is not efficient unless special measures are taken.[83,84] One of the effects associated with current heating is typically the loss in device efficiency as the enhanced temperature affects electrons and holes differently. While this effect is reversible, there could also be a thermal runaway[72] that would result in fast degradation, probably through hot spots. Such thermal runaway can be understood by considering that the current in proportional to the mobility $J_{SCL} = \frac{9}{8}\varepsilon\mu\frac{V^2}{d^3}$, and that the mobility is temperature dependent, as described in Equations 24 or 25: $\mu(E,T) = \mu_0 \exp\left[-\frac{\Delta}{kT} + B\left(\frac{1}{kT} - \frac{1}{kT_0}\right)E^{0.5}\right]$. To these, we need only to add the fact that the joule heating raises the device temperature above its heat-sink temperature (T_{HS}): $T = T_{HS} + IVR_T$. The lower limit for the effective thermal resistance (R_T), for most experimental configuration, would be close to that of the heat resistance of 1 mm^3 glass, which is 110 K W^{-1}, and the actual value could easily be 10 times higher.

Figure 33 shows the *j–V* characteristics derived by solving the three equations above self-consistently for a 1 mm^2 device. The full line is calculated for $R_T = 0$ K W^{-1}, the dashed-dotted line for $R_T = 160$ K W^{-1}, and the dashed line for $R_T = 1600$ K W^{-1}. We note that for the set of parameters used at around 10–15 V, the device temperature would rise by about 30–50 K, which would induce a catastrophic thermal runaway of the current and temperature. In practice, this thermal runaway would be less steep due to the presence of serial resistance, which is associated with the leads and contacts.

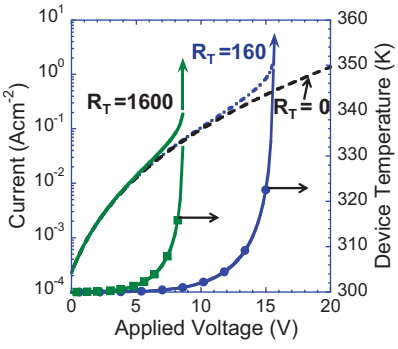

Figure 33. Calculation of the current density as a function of voltage for a 1 mm^2 device under constant-wave (CW) drive scheme and including joule heating effects. The full line is calculated for $R_T = 0$ K W^{-1}, the dashed-dotted line for $R_T = 160$ K W^{-1}, and the dashed line for $R_T = 1600$ K W^{-1}. $\mu_0 = 35$ cm^2 V^{-1} s^{-1}, $\Delta = 4.8$ eV, $B = 2.9 \times 10^{-5}$ eV, and $T_0 = 600$ K.

7. Summary

In this tutorial review, we have tried to describe several of the theories or approaches abundant in the literature concerned with charge transport. From the enormous number of contributions, we have tried to choose those which would help most to develop some intuition with respect to transport in organic-materials-based devices operating at, or not far from, room temperature. By nature, such a choice is highly subjective, and we hope that at least most of the important features were covered. In the first sections, we have also tried to emphasize that there is always more than what just meets the eyes (our "Behind the Scenes" sections), as this is extremely important in a material-driven field that is still evolving through the introduction of new materials, and where news specialists from different disciplines are joining and bringing new/different views and outlooks.

Acknowledgements

We acknowledge support of the Israel Science Foundation and the Russel Berry Nanotechnology Institute at the Technion (RBNI). We thank D. Natali for the fruitful comments.

Received: December 1, 2008
Revised: January 14, 2009
Published online: May 7, 2009

[1] N. W. Ashcroft, N. D. Mermin, *Solid State Physics*, Holt, Rinehart and Winston, New York **1988**.
[2] P. W. Anderson, *Phys. Rev.* **1957**, *109*, 1492.
[3] M. A. Lampert, P. Mark, *Current Injection in Solids*, Academic Press, New York **1970**.
[4] M. Pope, C. E. Swenberg, *Electronic Processes in Organic Crystals*, Clarendon Press, Oxford **1999**.
[5] A. Miller, E. Abrahams, *Phys. Rev.* **1960**, *120*, 745.
[6] N. F. Mott, W. D. Twose, *Adv. Phys.* **1961**, *10*, 107.
[7] T. Holstein, *Ann. Phys.* **1959**, *8*, 325.
[8] S. Guha, J. D. Rice, Y. T. Yau, C. M. Martin, M. Chandrasekhar, H. R. Chandrasekhar, R. Guentner, P. S. de Freitas, U. Scherf, *Phys. Rev. B* **2003**, *67*, 125204.
[9] S. Guha, J. D. Rice, C. M. Martin, W. Graupner, M. Chandrasekhar, H. R. Chandrasekhar, U. Scherf, *Mater. Res. Soc. Symp.* **2002**, BB10. 7.1.

[10] N. F. Mott, *Electronic Processes in Non-crystalline Materials*, Clarendon Press, Oxford **1979**.
[11] Y. Preezant, N. Tessler, *Phys. Rev. B* **2006**, *74*, 235202.
[12] M. Yan, L. Rothberg, B. R. Hsieh, R. R. Alfano, *Phys. Rev. B* **1994**, *49*, 9419.
[13] V. Ambegaokar, B. I. Halperin, J. S. Langer, *Phys. Rev. B* **1971**, *4*, 2612.
[14] M. Vissenberg, M. Matters, *Phys. Rev. B* **1998**, *57*, 12964.
[15] M. Vissenberg, Opto-Electronic Properties of Disordered Organic Semiconductors, Ph.D. Thesis, Universiteit Leiden, Leiden **1999**.
[16] D. Monroe, *Phys. Rev. Lett.* **1985**, *54*, 146.
[17] S. D. Baranovskii, T. Faber, F. Hensel, P. Thomas, *J. Non-Cryst. Solids* **1996**, *200*, 222.
[18] V. I. Arkhipov, P. Heremans, E. V. Emelianova, G. J. Adriaenssens, H. Bassler, *J. Phys. Condens. Matter* **2002**, *14*, 9899.
[19] H. C. F. Martens, I. N. Hulea, I. Romijn, H. B. Brom, W. F. Pasveer, M. A. J. Michels, *Phys. Rev. B* **2003**, *67*, 121203.
[20] N. Tessler, Y. Roichman, *Org. Electron.* **2005**, *6*, 200.
[21] Y. Roichman, N. Tessler, *Appl. Phys. Lett.* **2002**, *80*, 1948.
[22] S. D. Baranovskii, I. P. Zvyagin, H. Cordes, S. Yamasaki, P. Thomas, *Phys. Status Solid B Basic Res.* **2002**, *230*, 281.
[23] S. Shaked, S. Tal, Y. Roichman, A. Razin, S. Xiao, Y. Eichen, N. Tessler, *Adv. Mater.* **2003**, *15*, 913.
[24] Y. Roichman, Y. Preezant, N. Tessler, *Phys. Status Solidi A Appl. Res.* **2004**, *201*, 1246.
[25] Y. Roichman, Charge Transport in Conjugated Polymers, Ph.D. Thesis, Technion Israel Institute of Technology, Haifa **2004**, the thesis can be found at http://www.ee.technion.ac.il/labs/orgelect/ under ''published papers'' (Accessed on 1.3.2009).
[26] J. M. Ziman, *Models of Disorder*, Cambridge University Press, Cambridge **1979**.
[27] H. Bassler, *Phys. Status Solidi B* **1993**, *175*, 15.
[28] M. Van der Auweraer, F. C. Deschryver, P. M. Borsenberger, H. Bassler, *Adv. Mater.* **1994**, *6*, 199.
[29] H. Scher, E. M. Montroll, *Phys. Rev. B* **1975**, *12*, 2455.
[30] Z. G. Yu, D. L. Smith, A. Saxena, R. L. Martin, A. R. Bishop, *Phys. Rev. B* **2001**, *63*, 085202.
[31] D. M. Goldie, *J. Non-Cryst. Solids* **2000**, *266*, 294.
[32] J. Zhou, Y. C. Zhou, J. M. Zhao, C. Q. Wu, X. M. Ding, X. Y. Hou, *Phys. Rev. B* **2007**, *75*, 153201.
[33] W. F. Pasveer, J. Cottaar, C. Tanase, R. Coehoorn, P. A. Bobbert, P. W. M. Blom, D. M. de Leeuw, M. A. J. Michels, *Phys. Rev. Lett.* **2005**, *94*, 206601.
[34] Y. N. Gartstein, E. M. Conwell, *Chem. Phys. Lett.* **1995**, *245*, 351.
[35] S. V. Novikov, D. H. Dunlap, V. M. Kenkre, P. E. Parris, A. V. Vannikov, *Phys. Rev. Lett.* **1998**, *81*, 4472.
[36] S. V. Novikov, A. V. Vannikov, *J. Phys. Condens. Matter* **1994**, *6*, 10519.
[37] U. Wolf, H. Bassler, P. M. Borsenberger, W. T. Gruenbaum, *Chem. Phys.* **1997**, *222*, 259.
[38] H. Kageyama, K. Ohnishi, S. Nomura, Y. Shirota, *Chem. Phys. Lett.* **1997**, *277*, 137.
[39] A. Peled, L. B. Schein, D. Glatz, *Phys. Rev. B* **1990**, *41*, 10835.
[40] N. F. Mott, R. W. Gurney, *Electronic Processes in Ionic Crystals*, Oxford University Press, London **1940**.
[41] B. N. Limketkai, P. Jadhav, M. A. Baldo, *Phys. Rev. B* **2007**, *75*, 4.
[42] B. I. Shklovskii, E. I. Levin, H. Fritzsche, S. D. Baranovskii, in *Transport, Correlation and Structural Defects* (Ed.: H. Fritzsche), World Scientific, Singapore **1990**, p. 161.
[43] S. Marianer, B. I. Shklovskii, *Phys. Rev. B* **1992**, *46*, 13100.
[44] H. Scher, M. F. Shlesinger, J. T. Bendler, *Phys. Today* **1991**, *44*, 26.
[45] E. M. Horsche, D. Haarer, H. Scher, *Phys. Rev. B* **1987**, *35*, 1273.
[46] N. Rappaport, O. Solomesch, N. Tessler, *J. Appl. Phys.* **2006**, *99*, 064507.
[47] N. Rappaport, Y. Preezant, N. Tessler, *Phys. Rev. B* **2007**, *76*, 235323.
[48] I. N. Hulea, H. B. Brom, A. J. Houtepen, D. Vanmaekelbergh, J. J. Kelly, E. A. Meulenkamp, *Phys. Rev. Lett.* **2004**, *93*, 166601.
[49] V. I. Arkhipov, P. Heremans, E. V. Emelianova, H. Bassler, *Phys. Rev. B* **2005**, *71*, 45214.
[50] V. I. Arkhipov, E. V. Emelianova, G. J. Adriaenssens, *Phys. Rev. B* **2001**, *6308*, 081202.
[51] U. Pinsook, V. Sa-yakanit, *Solid State Commun.* **2008**, *148*, 42.
[52] O. Tal, Y. Rosenwaks, Y. Preezant, N. Tessler, C. K. Chan, A. Kahn, *Phys. Rev. Lett.* **2005**, *95*, 256405.
[53] O. Tal, Electronic Properties of Organic Thin Films Studied by Kelivn Probe Force Microscopy, Ph.D. Thesis, Tel-Aviv University, Tel-Aviv **2006**.
[54] J. Veres, S. D. Ogier, S. W. Leeming, D. C. Cupertino, S. M. Khaffaf, *Adv. Funct. Mater.* **2003**, *13*, 199.
[55] P. M. Borsenberger, H. Bassler, *J. Chem. Phys.* **1991**, *95*, 5327.
[56] O. Tal, I. Epstein, O. Snir, Y. Roichman, Y. Ganot, C. K. Chan, A. Kahn, N. Tessler, Y. Rosenwaks, *Phys. Rev. B* **2008**, *77*, 201201.
[57] R. A. Street, *Technology and Applications of Amorphous Silicon*, Springer-Verlag, Berlin **1999**.
[58] J. Kanicki, S. Martin, in *Thin-Film Transistors*, (Eds: C. R. Kagan, P. Andry), Marcel Dekker, New York **2003**.
[59] M. Shur, M. Hack, *J. Appl. Phys.* **1984**, *55*, 3831.
[60] L. Resendiz, M. Estrada, A. Cerdeira, *Solid-State Electron.* **2003**, *47*, 1351.
[61] G. Horowitz, P. Lang, M. Mottaghi, H. Aubin, *Adv. Funct. Mater.* **2004**, *14*, 1069.
[62] L. Fumagalli, M. Binda, D. Natali, M. Sampietro, E. Salmoiraghi, P. Di Gianvincenzo, *J. Appl. Phys.* **2008**, *104*, 084513.
[63] J. H. Werner, H. H. Guttler, *J. Appl. Phys.* **1991**, *69*, 1522.
[64] K. Maeda, *Surf. Sci.* **2001**, *493*, 644.
[65] V. I. Arkhipov, U. Wolf, H. Bassler, *Phys. Rev. B* **1999**, *59*, 7514.
[66] V. I. Arkhipov, E. V. Emelianova, Y. H. Tak, H. Bassler, *J. Appl. Phys.* **1998**, *84*, 848.
[67] D. F. Blossey, *Phys. Rev. B* **1974**, *9*, 5183.
[68] J. C. Scott, G. G. Malliaras, *Chem. Phys. Lett.* **1999**, *299*, 115.
[69] Y. Preezant, N. Tessler, *J. Appl. Phys.* **2003**, *93*, 2059.
[70] M. A. Baldo, S. R. Forrest, *Phys. Rev. B* **2001**, *6408*, 5201.
[71] B. N. Limketkai, M. A. Baldo, *Phys. Rev. B* **2005**, *71*, 085207.
[72] D. J. Pinner, R. H. Friend, N. Tessler, *J. Appl. Phys.* **1999**, *86*, 5116.
[73] D. J. Pinner, R. H. Friend, N. Tessler, *Synth. Met.* **2001**, *124*, 41.
[74] B. K. Crone, P. S. Davids, I. H. Campbell, D. L. Smith, *J. Appl. Phys.* **2000**, *87*, 1974.
[75] D. J. Pinner, R. H. Friend, N. Tessler, *J. Appl. Phys.* **2005**, *97*, 014504.
[76] N. Tessler, D. J. Pinner, V. Cleave, D. S. Thomas, G. Yahioglu, P. Lebarny, R. H. Friend, *Appl. Phys. Lett.* **1999**, *74*, 2764.
[77] D. J. Pinner, R. H. Friend, N. Tessler, *Appl. Phys. Lett.* **2000**, *76*, 1137.
[78] J. S. Kim, M. Granstrom, R. H. Friend, N. Johansson, W. R. Salaneck, R. Daik, W. J. Feast, F. Cacialli, *J. Appl. Phys.* **1998**, *84*, 6859.
[79] M. Kemerink, S. Timpanaro, M. M. deKok, E. A. Meulenkamp, F. J. Touwslager, *J. Phys. Chem. B* **2004**, *108*, 18820.
[80] B. J. Leever, M. F. Durstock, M. D. Irwin, A. W. Hains, T. J. Marks, L. S. C. Pingree, M. C. Hersam, *Appl. Phys. Lett.* **2008**, *92*, 013302.
[81] N. Rappaport, Y. Bar, O. Solomeshch, N. Tessler, *Appl. Phys. Lett.* **2006**, *89*, 252117.
[82] G. J. Adriaenssens, V. I. Arkhipov, *Solid State Commun.* **1997**, *103*, 541.
[83] N. Tessler, N. T. Harrison, D. S. Thomas, R. H. Friend, *Appl. Phys. Lett.* **1998**, *73*, 732.
[84] J. C. Sturm, W. Wilson, M. Iodice, *IEEE J. Selec. Topics Quantum Electron.* **1998**, *4*, 75.